Three waves of ovarian follicles in juvenile mice

Qi Yin[1] and Allan C. Spradling[1,*]

[1]Howard Hughes Medical Institute and Department of Biosphere Sciences, Carnegie Institution for Science, Baltimore, MD 21218, USA

[*] corresponding author and lead contact: spradling@carnegiescience.edu

Competing interests: The authors declare that no competing interests exist.

ABSTRACT

We characterized 3 waves of ovarian follicles in juvenile mice using tissue clearing, lineage tracing and scRNAseq. Wave 1 follicles grow with little delay, and express steroidogenic cell inducers by 2 weeks, as thecal and interstitial gland cells arise. Beginning at 3 weeks, >80% of wave 1 follicles degrade their oocytes, turn over most granulosa cells, and cluster together in the medulla. Thecal cells increase further around holes left by oocytes, and during puberty (5 wk), highly express androgen biosynthetic genes. "Boundary follicles" at the medullar-cortical boundary, comprise the earliest-activated wave 2 follicles. They express *Foxl2* as early as E14.5, and generate >70% of the first mature oocytes. Our results indicate the medulla's broad importance in initial follicular development, and argue that gamete waves, a common animal strategy, serve specific purposes. Wave 1 follicle derivatives bring about high androgen expression during puberty that likely impacts sex-specific neurodevelopment, while boundary and wave 2 follicles support early and lifelong fertility. Consistent with their distinct roles, granulosa cells of antral wave 1 and wave 2 follicles differentially express multiple genes, including *Wnt4* and *Igfbp5*.

SIGNIFICANCE STATEMENT

We studied the ovaries of juvenile mice 2-6 weeks (wk) of age using transcriptomics and cell lineage to characterize the earliest developing groups of follicles. "Wave 1" follicles begin growing at birth in the ovarian medulla (central region), but most do not produce mature oocytes. Instead they remodel to generate cells synthesizing androgens at puberty, which likely affect sex-specific neurodevelopment. A newly recognized group, "boundary follicles" activate next at the medulla-cortex boundary; their oocytes mature and give rise to most early offspring. The remaining "wave 2" follicles constitute the quiescent ovarian reserve and activate in small groups throughout later life. Our results highlight the importance of specific spatially-localized follicle subgroups and show that they aid reproduction in distinct ways, some of which involve extensive cellular remodeling.

INTRODUCTION

Despite significant differences in the organization of mammalian gonadal primordia, gametes often begin development in subgroups known as "waves" that arise at specific times and gonadal locations (Browning, 1973; Hirshfield, 1992; Gougeon, 1996; Jiménez, 2009; DeFalco and Capel, 2009; Rotgers et al. 2018). Yet the reasons waves exist are poorly understood, and some appear to generate gametes that mostly turn over by atresia (Hsueh et al. 1994). In mice, the earliest developing follicles, known as "wave 1," develop in the ovarian medulla and begin maturation with little arrest shortly after birth. The remaining 90%, "wave 2," enter quiescence by forming primordial follicles within the ovarian cortex before postnatal day 5 (P5) (Figure 1A). Different somatic granulosa cells cover wave 1 and 2 follicles. In the medulla, wave 1 follicles retain early arising bipotential granulosa cells (BPGs), which express *Foxl2* during early fetal development, whereas wave 2 follicles in the cortex acquire epithelial granulosa cells (EPGs) and express *Foxl2* later and at lower levels (Hirshfield, 1992; Mork et al., 2012; Zheng et al. 2014a,b; Niu and Spradling, 2020). All wave 1 follicles and a few wave 2 primordial follicles express *Nr5a2* (Niu and Spradling, 2020; Meinsohn et al. 2021a).

Most wave 1 follicles undergo atresia after reaching early antral stages (Byskov et al. 1974; Erickson et al. 1985) during juvenile development (Figure 1B). This suggests they do not serve a direct reproductive function (Hirshfield, 1992; Hseuh et al. 1994; Eppig and Handel, 2012), although these follicles are capable of developing into functional oocytes following superovulation (Lamas et al. 2021). In contrast, small groups of wave 2 follicles periodically activate beginning no earlier than 2 weeks after birth (Zheng et al. 2014a,b), and grow in response to nutritional and regulatory signals to sustain lifelong fertility (reviews: Edson et al. 2009; McKey et al. 2022). Surprisingly, tagging *Foxl2*-positive granulosa cells using *Foxl2*-CreER^{T2} at E16.5 efficiently labeled wave 1 follicles and showed that many of the marked

follicles survive and contribute offspring during the initial months of fertility (Zheng et al. 2014a). This suggested that wave 1 follicles were an extremely inefficient way to make the first ovulated follicles.

Once activated in primary follicles, granulosa cells (GCs) start to proliferate and soon form multiple GC layers surrounding the oocyte (Habara et al., 2021; Figure S1A-D). Granulosa cells in secondary follicles send signals encoded by Desert hedgehog (*Dhh*) and Indian hedgehog (*Ihh*) that attract ovarian mesodermal precursors to form outer thecal cell layers on follicles and to synthesize steroid hormones (review Richards et al. 2017). Additionally, ovarian medullary precursors generate thecal fibroblastic cells and perivascular smooth muscle cells that vascularize the thecal region and enable such follicles to collectively serve as a major systemic steroid hormone source (Guzmán et al. 2023). An ovarian cell type closely related to thecal cells, interstitial gland cells, also coordinately form in mice and many other mammals (Jiménez, 2009; Miyabayashi et al. 2015). *Nr5a2* promotes thecal cell vascularization that is essential for ovulation (Duggavathi et al. 2008; Bianco et al. 2019; Guzmán et al. 2022). Two classes of steroid hormone-producing Leydig cells, fetal and adult, also arise during testis development (Miyabayashi et al. 2015; Liu et al. 2016).

Follicular cells synthesize specific steroid hormones during their development (Richards et al. 2017; Niu and Spradling, 2020; Meinsohn et al. 2021b). Thecal steroidogenic cells of late secondary and preantral follicles convert cholesterol to androgens through a series of enzymatic reactions involving steroidogenic acute regulatory protein (StAR), cytochrome P450 family 11 subfamily A member 1 (CYP11A1), hydroxy-delta-5-steroid dehydrogenase, 3 beta- and steroid delta-isomerase 1 (HSD3B1), cytochrome P450 family 17 subfamily A member 1 (CYP17A1), and steroid 5 alpha-reductase 1 (SRD5A1). Ovarian androgen production by thecal cells during juvenile development is essential for normal maturation and puberty onset (Galas et al. 2012;

Walters et al., 2019; Kelava et al., 2022). In addition, thecal androgens diffuse into neighboring GCs, where they are converted into estrogen by the action of hydroxysteroid 17-beta dehydrogenase 1 (HSD17B1) and cytochrome P450 family 19 subfamily A member 1 (CYP19A1). Estrogen produced in this manner signals the hypothalamus to initiate gonadotrophin production and is essential for subsequent follicular maturation. After ovulation, the oocyte-free follicle is further modified into a corpus luteum, and its thecal cells undergo luteinization to generate progesterone (Edson et al. 2009).

We investigated the development of follicles in 2-6 wk mouse ovaries in detail using scRNAseq and lineage tracing to better understand the role of gamete waves and follicular atresia. We find that the wave 1 follicles undergo developmental remodeling rather than generic atresia and characterize distinct gene expression programs of their granulosa and thecal cells, as well as of wave 2 follicular and stromal cells during juvenile development. Moreover, we identify a small subset of wave 2 primordial follicles (~400 out of >2,000) exclusively located at the cortex-medullar boundary as the major source of the earliest fertile oocytes, rather than wave 1 follicles. These results suggest that wave 1 follicles remodel to promote high juvenile androgen production and do not undergo exceptionally levels of atresia due to developmental defects. It is likely that all three follicular waves are optimized to maximize reproductive success under natural environmental conditions.

RESULTS

Wave 1 follicle development

Advances that allow tissue clearing (Faire et al., 2015; Feng et al., 2017; Fiorentino et al., 2020; McKey et al., 2022), make it possible to image the entire mouse ovary without sectioning. To better understand wave 1 follicle development, we employed a clearing-enhanced 3D (C_e3D) method to analyze wild type C57BL/6J ovaries at the cellular level after whole-mount staining

(Li et al., 2017) as well as analyzing sectioned material (Figure S1). Multiple ovaries were reconstructed during weeks (wk) 1-5 of development (Table S1). In C57BL/6J mice, puberty (peri-puberty) typically occurs between 4 and 5 wk of age, but the first ovulation, which signals sexual maturity, doesn't take place until 7 wk (Figure 1B) (Nelson et al., 1990; Zhou et al., 2007).

Using these tools we characterized the development of wave 1 follicles in detail. Wave 1 follicles begin to grow as primary follicles near the time of birth based on gene expression (Niu and Spradling, 2020). By P10 we counted about 3,300 total follicles (Figure 1C; Figure S1E-G) and 278-293 wave 1 follicles (Figure 1D; Figure S1E-G); wave 1 oocyte volume increased during wk 1-wk3 (Figure 1E). By 2 wk, many wave 1 follicles in the medulla contained 2-4 layers of GCs and 1-2 thecal cell layers, appearing as normal secondary or antral follicles (Figure S1A-D, G) .

Wave 1 follicles undergo atresia-like remodeling

By 3 wk, wave 1 follicles begin to remodel, changes that have traditionally been attributed to whole follicle degeneration known as "atresia" (Figure S2; Table S1; Supplemental Movies). These follicles were first identified due to oocyte loss, initially leaving behind nearly intact granulosa and thecal cell layers (Figure 1F; Figure S2A,B). The non-canonical follicles become reduced in size and retain a hole beneath the granulosa cell layer where the oocyte had been located. Oocyte loss from wave 1 follicles increases further by 4 weeks, and exceeds 80% by 5 wk (Figure S2A,B; Figure 1F). Examination in the electron microscope revealed that the holes retain the oocyte's zona (ZP) for a considerable period, which may stabilize them (Figure S2B). We confirmed that these events also occur in the DBA/2J strain (Figure S2C). Thus, the great majority of wave 1 follicles lose their oocytes prior to puberty and do not contribute to early ovulation.

The loss of oocytes from most wave 1 follicles was not due to non-specific atresia, as expected if these follicles contained developmental or meiotic defects. Instead, the remodeling appears to be a developmental process in which thecal cells are retained while oocytes and most granulosa cells are lost. Documenting the nature of wave 1 follicle remodeling was assisted by tracing cell lineages. We used *Foxl2*-CreER^{T2} mice to selectively lineage label GCs associated with wave 1 follicles (Figure 2A; Mork et al. 2012; Zheng et al. 2014a) and to follow their behavior during follicle remodeling (Figure 2). Following brief administration of Tamoxifen (TAM) at embryonic day 16.5 (E16.5), most wave 1 follicles showed mosaic EYFP-labeling of GCs at 2 wk while nearly all cortical wave two follicle granulosa cells were unlabeled (Figure 2B, C). By 5 wk the number of follicles with DDX4-positive oocytes and normal granulosa layers had decreased to a mean of 26 (Figure 2D, E). Remodeled follicles lost 94% of their granulosa cells compared to 3 wk wave 1 follicles prior to remodeling, retaining only 6% (14/255), located adjacent to the hole (Figure 2F). When similar lineage labeling was carried out at 5 wk and analyzed at 6 wk, the number of labeled granulosa cells in remodeled follicles remained low and in the same location (Figure 2G). As part of remodeling, wave 1 oocyte holes decreased in size and remodeled follicles clustered in the medulla (Figure 2F, arrowheads; Figure S2A,B).

Identification of an early activating subpopulation of primordial follicles

Lineage tracing experiments also identified a new subclass of primordial follicles located near the medulla-cortex boundary (Figure S3). Whether assayed with tdTomato (Figure S3A-D) or EYFP (Figure S3E-G), *Foxl2*-CreER^{T2} activation by TAM injection at E16.5 labels not only wave 1 medullar follicle GCs, but at 2 wk it labels a small subset of primordial follicles near the cortex-medulla boundary that contain 1 or a few positive granulosa cells (Figures S3C-E). A mean of 421 such "boundary" follicles were identified among 5,843 total follicles (Figure S3F).

Boundary follicles begin to develop shortly after 2 wk since nearly 70% of normal secondary follicles in 5 wk ovaries contained EYFP-positive GCs (Figure S3G). More than 70% of pre-antral or later follicles also contained EYFP GCs up to at least 5 wk (Figure S3H,I). A small number of primordial follicles containing one or a few EYFP-positive GCs appeared at the medulla/cortex boundary even when TAM was injected at E14.5, rather than E16.5 (Fig. S3J).

Developing wave 1 follicles retain thecal cells and expand their number

Further lineage marking revealed the behavior of steroidogenic thecal cells (STCs) that remain associated with remodeling wave 1 follicles (Figure 3). We validated that thecal cells strongly express the steroid biosynthetic enzyme CYP17A1 at 3 wk using immunofluorescent staining (Figure S4A). Consequently, we used the *Cyp17a1* gene to drive optimized Cre (iCre) and activate CAG-tdTomato (Figure 3A) to mark STCs. In 2 wk ovaries, tdTomato expression was observed in thecal cells sheathing large medullar follicles (Figure 3B,C). Additional cells that appear to be interstitial gland cells also become labeled between many follicles (Figure S4B,C; arrows). During wave 1 follicle development from 2 ws to 5 wk, the number of tdTomato-labeled cells associated with nuclear holes dramatically increases (compare Figure 3D to 3E). Some granulosa cells (GCs) may also become labeled initially (Figure S4C, arrowheads) perhaps because GC precursor cells briefly express *Cyp17a1* during embryonic stages. Because, most GCs turn over as part of wave 1 remodeling (Figure 2D) the multiple, nearly uniform groups of tdTomato-positive cells associated with remodeled wave 1 follicles by 5 wk represent abundant STCs and interstitial gland cells containing subcellular features associated with steroid production. Oil red staining documented abundant lipid droplet accumulation in these cells from 2 wk to 5 wk (Figure 3F,G). These cells express the steroidogenic proteins HSD3B1, and PLIN1 (Figure 3H). Electron microscopy confirmed that expanded wave 1 follicular cells display distinctive lipid droplets and mitochondria characteristic of thecal and interstitial gland cells

(Figure 3I; Figure S4D). Wave 1 follicle remodeling by 5 wk has generated a cellular cluster within the medulla (Figure 3J), which persists within the ovary after 5 wk (Figure S4E).

Mapping cell transcription during wave 1 remodeling

To gain more insight into wave 1 follicle development and remodeling, we analyzed gene expression in single cells from ovaries every wk from wk2 to wk6 (Figure 4A; Supplemental Datasets S1-S6). 31 initial clusters (c0-c30) were identified, comprising nine major cell group (Figure 4A'), based on their expression of well known marker genes (Figure S5A,B). These comprised granulosa cells (*Amhr2*, Poole et al., 2016), stromal cells (*Mfap4*, Morris et al., 2022), thecal cells (*Cyp17a1*, Young and McNeilly, 2010), hematopoietic cells (*Runx3*, Boto et al., 2018), endothelial cells (*Cldn5*, Richards et al., 2022), pericytes (*Notch3*, Wang et al., 2014), smooth muscle cells (*Acta2*, Rockey et al., 2013), and epithelial cells (*Upk3b*, Niu and Spradling, 2020). Four clusters exhibited low UMIs, and were excluded them from subsequent analysis, as was cluster14 due to the presence of suspected doublets. Because germ cells make up only a small fraction of the total cell population, a germ cell cluster was not detected.

The initial clustering further validated the picture of wave 1 development obtained from lineage studies. Cluster c1 expressed wave 1 BPG granulosa cell markers like *Nr5a2*, *Hsd3b1*, *Inha*, *Inhba* and increased 4-fold in cell number between wk2-wk4, before falling at wk 5 as wave 1 granulosa cells turn over (Supplemental Dataset S6). Cluster c16 highly expressed thecal cell steroidogenic genes such as *Cyp11a1*, *Cy17a1*, and *Plin1*. The number of c16 cells peaked at puberty (wk5). The outer "theca externa" is enriched in angiogenic cells, blood vessels, and fibroblastic cells. Clusters corresponding to endothelial cells expressing *Flt1* (c22) and blood cells expressing *Laptm5* (c23), increased nearly 4-fold between wk3 and wk5, consistent with such vascularization.

We re-clustered the ten initial granulosa cell (GC) clusters (Figure 4A') in Seurat, yielding 18 new clusters gc0-gc17; (Figure 4B) and classified them into groups corresponding to their likely association with primordial (gc11), primary (gc3, gc8), secondary (gc1, gc4, gc9), antral (gc2, gc7, gc10, gc13), and remodeling (gc0, gc6) follicles, as well as mitotically cycling cells (Figure 4B'; Figure S5C). We also re-clustered the mesenchymal and stromal cells (Figure 4A') yielding 21 new clusters to pursue a higher resolution picture of thecal expansion (Figure 4C; Figure S5D). The re-clustered mesenchymal cells fell into eight groups, STCs expressing *Cyp17a1*, *Tagln*-expressing fibroblasts (Sun et al., 2023), *Col14a1*-expressing fibroblasts (Xie et al., 2018), *Cd24a*-expressing fibroblasts (Wang et al., 2022), *Cxcl12*-expressing fibroblasts (Sjöberg et al., 2019), *Hoxd9*-expressing fibroblasts (Khoa et al., 2001), *Col11a1*-expressing fibroblasts (Zhang et al. 2023) and mitotic cells expressing *Mki67* (Figure 4C, C'). We identified up to 250 top differentially expressed genes for each group (Supplemental Dataset 5) to enable Metascape Analysis (Zhou et al. 2019). The development and remodeling of wave 1 follicles, and of boundary follicles giving rise to early wave 2 follicles is summarized in Figure 5.

Comparing gene expression in wave 1 vs wave 2 follicle development

The separation of wave 1 and wave 2 follicles begins early in fetal development, as BPG and EPG granulosa cells begin to express different genes as early as E14.5 and diverge further by P5 (Niu and Spradling, 2020). To investigate whether gene expression differences at follicle formation persist and to look for additional wave-specific gene expression, we examined granulosa cell clusters gc2, gc7, gc10 and gc13 at 2wk, comprising all GC clusters scored as in antral follicles (Figure 4B'). As illustrated in Figure 5, only "normal" wave 1 antral follicles are present in significant numbers at wk2 and wk3, prior to widespread wave 1 remodeling. In contrast, because of extensive wave 1 granulosa cell turnover, by wk 5 nearly all these same antral follicle clusters come from developing wave 2 boundary follicles. Consequently we

compared gene expression levels during these two time intervals for all four antral granulosa cell clusters.

The nuclear receptor *Nr5a2*/*Lrh1*, is preferentially expressed 7.8-fold higher in P5 BPGs than EPGs (Niu and Spradling, 2020); similarly, expression is 11-fold higher in 2wk antral compared to primordial follicle (gc11) granulosa cells. However, this difference probably reflects the early activation of wave 1, as *Nr5a2* turns on at lower levels in all wave 2 granulosa cells as they begin to grow (Meinsohn et al. 2019) and we observed that it increases in primary and secondary follices, reaching similar levels in wave 1 and wave 2 antral follicles (ratio = 1.02+/- 0.23). Comparable expression ratios were likewise seen between wave 1 and wave 2 antral granulosa cells for other BPG-preferential genes including *Dhh* (1.04+/- 0.41), *Hsd17b1* (0.61+/- 0.14), *Ptgis* (1.08+/- 0.26), *Prlr* (1.8+/- 0.80), *Fshr* (0.89+/- 0.21) and *Igf1* (0.86+/- 0.10). When we looked at all genes (expressed at >1 tpm), however, significant differences were seen. Wave 1 wk2 antral GCs express *Wnt4* at much higher levels (4.8 +/- 1.0) compared to Wave 2 antral CGs at either wk 5 (0.17 +/- 0.069) or wk 6 (0.14 +/- 0.070). Other genes expressed more highly in wave 1 than wave 2 are *Igfbp5* (ratio: 27 +/- 10); *Itga6* (ratio: 6.28 +/- 0.97) and *Inha* (ratio: 1.52 +/- 0.29). Genes expressed a lower levels in wave 1 than wave 2 include: *Cald1* (ratio: 0.20 +/- 0.089), *Ghr* (ratio: 0.16 +/- 0.027), *Grb14* (ratio: 0.23 +/- 0.092), and *Mmp11* (ratio: 0.46 +/- 0.23). Thus, gene expression is not entirely equivalent in wave 1 and wave 2 follicles at corresponding stages, as has often been assumed.

Clusters gc0 and gc6 showed indications they derived from remodeling wave 1 follicle. For example, the number of gc0 and gc6 cells is low at 2 and 3 wk but jumps 9.8-fold at wk 4 (Supplemental Dataset 6). Preferentially expressed genes in gc0 and gc6 include *Cyp1b1*, *Atf3*, *Cxcl1*, *Bmp2*, *Apoe* and *Sox4*. Metascape analysis identified vasculature development (-7.7; -4.0) cell cycle (-6.7; -9.2) , and positive regulation of programmed cell death (-4.1; nd), where

the numbers indicate (q values log10 for gc0; gc6). These findings suggest genes and pathways that GCs on remodeling wave 1 follicles use to stimulate vasculature development, and ultimately to promote GC population turnover during wk4.

Wave 1 STCs express a full set of androgen biosynthetic genes during puberty

Two clusters were identified as thecal cells, g9 and g11, due to expression of *Nr5a1* (Miyabayashi et al. 2015) and androgen biosynthetic genes (Figure 4D). g9 cells, strong candidates as follicular STCs, increased 4.1-fold between wk3 and wk5, while g11 cell number remained nearly constant (Supplemental Dataset 6). STCs expressing *Cyp11a1*, *Hsd3b1*, and *Cyp17a1*, increased in number from 2 wk to 5 wk, consistent with the *Cyp17a1* lineage tracing and staining results. *Star*, a crucial gene responsible for transporting cholesterol from the cytoplasm into mitochondria, is essential for steroidogenesis. The percentage of STCs expressing *Star* increased from approximately 50% to over 80% at wk 5 (Figure 4D). Our findings demonstrate that STCs increase in number, and acquire a full complement of androgen biosynthetic enzymes during peri-puberty. In contrast, granulosa cells expressing *Hsd3b1*, *Cyp19a1*, and *Hsd17a1* indicating the potential to synthesize estrogen peaked at wk 6 (Figure 4D), consistent with estrogen levels lagging androgen levels during puberty (Galas et al. 2012; Trova et al. 2021).

DISCUSSION

Wave 1 follicular remodeling generates a unique cluster of androgen-producing cells in the juvenile mouse ovary

Our work characterizes in detail the development of the first wave of mouse ovarian follicles at the cellular and gene expression levels. In agreement with earlier studies (Hirshfield and DeSanti, 1995; Gougeon 1996; McGee and Hsueh, 2000; Eppig and Handel, 2012), 80-100% of these follicles turn over rather than generating fertilizable oocytes. We characterize the

remodeling process they undergo that generates a sizable mass of thecal and interstitial gland steroidogenic cells located in the ovarian medulla by wk 5. mRNA analysis, antibody staining and tissue histology all show that these cells become highly active in androgen biosynthesis at this time and must contribute substantially to the high androgen levels present in female mice during puberty. By carrying out scRNAseq studies from wk2 to wk6, we were able to characterize the transcriptomes and identify many specific cell clusters that are involved in wave 1 follicle development, in the formation and amplification of steroidogenic cells, and in subsequent early wave 2 follicular development, all of which occur in or adjacent to the medulla. This work lays the groundwork for comparative studies of wave 1 with wave 2 follicular development, with corpus luteum remodeling, and with follicular atresia induced by developmental arrest or environmental stress. Moreover, it will encourage study of why some animals, such as mice, produce interstitial gland cells, while others such as sheep do not (Jiménez, 2009; Miyabayashi et al. 2015).

Early activating wave 2 "boundary follicles" provide most of the earliest mature oocytes

Previous lineage marking of *Foxl2*-expressing granulosa cells with GFP at E16.5 showed that follicles with labeled granulosa cells, presumed to be entirely of wave 1 origin, constituted all antral or older follicles up to sexual maturity (Zheng et al. 2014a). Many of these follicles ovulated during the first two months of fertility suggesting that wave 1 follicles contribute substantially to offspring even as they are gradually replaced by wave 2-derived follicles (Zheng et al. 2014a; review Zheng et al. 2014b).

The results presented here are consistent with the experimental data of Zheng et al. 2014a) but lead to a modified conclusion (Figure 5A). In addition to 225-250 wave 1 follicles in the medulla that begin rapid growth at birth, we identified about 400 wave 2 primordial follicles near the medullar-cortical border that are labeled with *Foxl2*-CreER^{T2} at E16.5 and begin to

activate as primary follicles by 2 wk. These appear to be similar or identical to a primordial follicle subclass located at the medulla/cortical boundary and expressing *Nr5a2* (Meinsohn et al. 2021a). Boundary follicles may activate before most other wave 2 follicles because their location at the medullary boundary close to wave 1 weakens quiescence, leading to early *Nr5a2* and *Foxl2* expression. Future studies will be required to clarify if early activating boundary follicles always contain *Nr5a2*-expressing granulosa cells, when it turns on, and whether these granulosa cells originate as EPGs, BPGs or both.

Regardless of the mechanism, boundary follicles as well as wave 1 follicles were labeled in our *Foxl2* lineage tracing experiments, and presumably those of Zheng et al. 2014a. Boundary primordial follicles activate as early as 2 wk and produce most of the first follicles to develop fully, ovulate and generate offspring (Figure S3). It remains possible that a small number of wave 1 follicles, ~25 or fewer, resist remodeling and also develop to maturity. However, based on oocyte turnover, their contribution to fertility, appears to be minor. Thus, early activated wave 2 follicles rather than wave 1 follicles are responsible for most early fertility. Most non-boundary wave 2 follicles may only begin to activate between puberty and sexual maturity, possibly in concert with the onset of pulsatile HPE axis activity.

The production of special boundary follicles that generate the earliest fertilizable oocytes indicates that the early developing wave 1 and the earliest developing wave 2 follicles both arise in or very close to the medulla. The more vascularized nature of the medulla may promote early development or inhibit quiescence establishment, and the mechanism of this influence will be important to understand. It would be interesting to see whether border follicle production varies in species that differ in the timing of female fertility onset.

Induction and functions of wave 1 follicles

Why most wave 1 follicles begin to develop rapidly, but break down without forming oocytes has been attributed to a variety of factors. Low levels of gonadotrophins in young juvenile mice have been suggested to prevent development past the preantral stage leading to non-specific wave 1 atresia (reviewed in Edson et al. 2009). However, the realization that these two follicular waves contain granulosa cells of different origin, and that BPGs and EPGs express many genes differentially throughout fetal development, supported the view that these follicles serve distinct developmental roles (Niu and Spradling, 2020). Here we have provided further evidence concerning wave 1 function, by showing that the "atresia" undergone by wave 1 follicles more closely resembles a development program of remodeling that amplifies production of steroidogenic thecal and interstitial gland cells. These cells expand further in number between wk 4 and wk 5 and cluster together in the ovarian medulla, suggesting that a major function of wave 1 is androgen production. Consistent with this, we show for the first time that wave 1 and wave 2 follicles express some genes differentially at comparable points in their development, early antral stages.

We explored conditions that reduce the number of wave 1 follicles in order to look for possible consequences. In Turner syndrome, wave 1 follicle development is significantly reduced (Miura et al. 2017). This imbalance might might decrease androgen levels, potentially affecting juvenile development. Consistent with hormonal disruption, hormone replacement therapy significantly improves the development of individuals with Turner syndrome (Klein et al., 2018). Moreover, androgens are known to play an important role in this effect (Zuckerman-Levin et al., 2009; Viuff et al., 2022).

We examined mouse X/O individuals and looked for changes in wave 1 follicle numbers (Figure S6B-C). In our experiments, wave 1 follicle numbers were reduced relative to levels in X/X control females at wk1 of development. However, the reduction was transient and by 2 wk,

before remodeling and thecal cell expansion, X/O and X/X females had regained a similar number of wave 1 follicles. Consequently, we could not draw any conclusions regarding the functional role of wave 1 follicles and their remodeling.

The normal fate of the wave 1 thecal network after puberty is also of considerable interest, since high relative androgen levels do not normally persist during adulthood (Trova et al. 2021). The scRNAseq data showed that androgen biosynthetic enzyme mRNAs per thecal cell decreased by 6 wk. However, thecal network cells likely remain since *Cyp17a1* lineage marking persisted in the medulla at least until wk 7 (Figure S4D). Non-border wave 2-derived follicles constitute 10% of growing follicles (but 0% of antral follicles) at puberty and 20% of growing follicles at sexual maturity (Zheng et al. (2014a). The decrease in androgenic enzymes without reduced cell numbers suggests that androgen production is downregulated after puberty.

Steroid hormones mediate sexual development in juvenile mice and during peri-puberty

Steroid hormones influence the development of sexually dimorphic organs including the brain (review Simerly, 2002; Arnold, 2009). They have multiple sources, including steroids in the maternal circulation during pregnancy, as well as subsequent systemic and local steroid production during juvenile stages. Wave 1-derived thecal cell numbers are high during wk 4-5 of juvenile development. a period known as peri-puberty that has been associated with sexual behavior development and with high levels of androgens, as well as relatively low estrogen production (Francois et al. 2017; Trova et al. 2021; Devillers et al. 2023). While the sensitivity of the brain to steroid influences is probably declining during this period, sexually dimorphic circuits are still being shaped in a manner that is important for sexually dimorphic behaviors in female and male rodents (Sisk and Zehr, 2005; Templin et al. 2019; Trova et al. 2021; Yoest et al. 2023). Potential targets of this influence include the anteroventral periventricular nucleus (AVPV) which is larger in female than male rodents, and helps regulate female reproductive

functions such as ovulation and gonadotrophin production. Sex hormones produced in females during puberty also enhance cell death in the primary visual cortex, reducing its volume in females compared to males.

Multiple gametic waves with differing outcomes are common in not only in mammals, but in diverse animal groups

The development of undifferentiated animal gonads into their adult forms varies even between related species and can be remarkably plastic in leading to production of male, female or both types of gametes in processes dependent on chromosome constitution or environment (DeFalco and Capel, 2009; Jiménez, 2009). Our studies of wave 1 follicle development represent a relatively simple example of such waves. An initial wave of germ cells in the mouse testis also develop during juvenile stages without generating mature gametes (Lei and Spradling, 2013). Two classes of steroid hormone-producing Leydig cells, fetal and adult, also arise in the developing testis (Miyabayashi et al. 2015; Liu et al. 2016). In many species of, the fate of gamete waves is plastic (Adolfi et al. 2023), and differential development of waves can lead to hermaphroditic gonads (McCarter et al. 1997).

Follicles in the human begin developing, as in mouse, long before there is any prospect of ovulation. Puberty in human females typically commences between the ages of 8 to 13 years, whereas antral follicles are present even in human fetuses and infants just a few months old and continue to be produced during juvenile life. Early follicles in humans, like in mice, might undergo remodeling to enhance production of androgens or other steroid hormones that sex-specifically influence organ and brain development (Cui et al., 2013; Bell, 2018). Detailed understanding how mouse wave 1 follicles develop is likely to be valuable in gaining a better understanding of these events.

Wave 1 follicle remodeling, polycystic ovarian syndrome and human follicular waves

The work reported here may be relevant to the origin and high frequency of polycystic ovary syndrome (PCOS) (McCartney and Marshall, 2016). Mouse wave 1 follicles dominate juvenile follicle development and generates a PCOS-like state by remodeling into cyst-like structures (i.e. lacking oocytes) with reduced granulosa layers but expanded thecal cells and interstitial gland cells producing androgens. Some of these characteristics of remodeling mouse wave 1 follicular resemble follicles within the ovaries of individuals with PCOS (Chang, 2007; Franks and Hardy, 2010; review- Walters et al. 2019).

However, to learn if PCOS is related to a problem in the developmental waves of juvenile human ovarian development will require that multiple important questions first be addressed. In the mouse, lineage labeling showed that many of wave 1-generated thecal cells remain after wk 5, but their androgenic enzymes mRNAs decrease by 6 weeks. Moreover, cells capable of estrogen production increased at 6 wk and likely require a source of androgens for conversion. How this reduction is controlled and how the increase in androgenic cells at puberty is terminated need to be understood.

MATERIALS AND METHODS

Experimental mice

All animal experiments were conducted in compliance with the Institutional Animal Care and Use Committee guidelines of the Carnegie Institution of Washington (CIW). The mice were housed in specific pathogen-free facilities at CIW. The strains of mice used in the study were acquired from Jackson Laboratory, including C57BL/6J (B6, strain #: 000664), DBA/2J (DBA2, strain #: 000671), B6;129P2-*Foxl2*$^{tm1(GFP/cre/ERT2)Pzg}$/J (*Foxl2*-CreER^{T2}, strain #: 015854), STOCK XO/J (XO, strain #: 036414), and B6;SJL-Tg(Cyp17a1-icre)AJako/J (*Cyp17a1*-icre, strain #: 028547). The R26R-LSL-EYFP reporter mice B6.129X1-*Gt(ROSA)26Sor*$^{tm1(EYFP)Cos}$/J (R26R-EYFP, strain #: 006148) were acquired from Jackson Laboratory and raised in a 129S1/SvImJ (129S1, strain #: 002448) background in our lab. The R26R-LSL-tdTomato (R26R-tdTomato) reporter mice were generously provided by Chen-Ming Fan at the CIW. CD-1 IGS Mouse (strain #: 022)was acquired from Charles river laboratories.

Lineage tracing experiments

To visualize the expression patterns of *Foxl2* and *Cyp17a1*, we generated reporter mouse lines by crossing R26R-EYFP or R26R-tdTomato mice with *Foxl2*-CreERT^2 or *Cyp17a1*-iCre (Shimshek et al., 2002; Zhou et al., 2022) mice. The presence of a vaginal plug was designated as embryonic day 0.5 (E0.5). Pregnant females were injected intraperitoneally (IP) with 1 mg tamoxifen (TAM) (MilliporeSigma, #T5648, 10 mg/ml dissolved in corn oil) per 35 g body weight at E16.5 or E14.5 (*Foxl2*-CreER^{T2}). The pups were delivered by C-section and fostered by a CD1 female mouse if they were not born late at night on the expected delivery day. The day of birth was considered postnatal day 0 (P0). We collected gonads from fetuses or ovaries from pups at the indicated stages for analysis. All experiments were conducted and analyzed on at

least two litters. The loss of one allele of *Foxl2* in *Foxl2*-CreER^{T2} and the administration of tamoxifen do not affect the ovarian development or overall mouse health.

To investigate the expression of *Foxl2* in remodeling follicles, tamoxifen was injected IP at a concentration of 1 mg/35 g into female mice at 5 weeks of age. The ovaries were dissected one week later and subjected to whole mount staining for analysis.

Immunostaining

For whole mount staining, gonads or ovaries were first fixed in 4% paraformaldehyde (PFA) in PBS overnight at 4°C. The tissues were then washed three times in a washing buffer (0.3% Triton X-100 and 0.5% thioglycerol in PBS) and incubated in blocking buffer (1% normal donkey serum, 1% BSA, and 0.3% Triton X-100 in PBS) overnight at 37°C. The samples were incubated with primary antibody in dilution buffer (1% BSA and 0.3% Triton X-100 in PBS) for two days at 37°C. After washing in the washing buffer overnight at 37°C, the samples were incubated with secondary antibodies in dilution buffer for another two days at 37°C, followed by washing in the washing buffer with DAPI overnight at 37°C. To increase transparency, the clearing buffer Ce3D (4g Histodenz in 2.75 ml 40% (v/v) N-methylacetamide) was then applied for another day. The samples were imaged using a Leica TCS SP8 confocal microscope or a Leica Stellaris 8 DIVE confocal microscope. Images were analyzed using Fiji or Imaris.

For cryosection staining, the dissected tissues were fixed in 4% PFA overnight at 4°C. After washing three times in PBS, the tissues were dehydrated sequentially in 10% and 30% sucrose solutions and embedded in O.C.T. for cryosectioning. The slides were sectioned at a thickness of 5 µm and stored at -20°C until staining. After antigen retrieval with 0.01% sodium citrate buffer, the slides were blocked for 1 hour at room temperature, incubated with primary antibodies overnight at 4°C, and then with secondary antibodies for 1 hour at room temperature. This was followed by counterstaining with DAPI for ten minutes before fixing in mounting

medium. The samples were then imaged with an upright SP5 microscope, and the images were analyzed using Fiji.

Oil Red O Staining

Oil Red O Staining was performed according to the protocol provided by Abcam (ab150678). Briefly, the slides were placed in propylene glycol for 5 minutes at room temperature, followed by incubation in Oil Red O solution at 60°C for 10 minutes. The slides were then differentiated in 85% propylene glycol for 1 minute, followed by rinsing twice in distilled water. The slides were then incubated in hematoxylin for 1 minute, and rinsed thoroughly in tap water and twice in distilled water. The slides were ready for imaging after applying a coverslip using an aqueous mounting medium. Imaging was done using a Nikon Eclipse E800 microscope.

Genotyping

The tissue was cut and placed in a lysis buffer (30 mM Tris-HCl, 0.5% Triton X-100, 20 µg/ml Proteinase K) and incubated at 55°C in a water bath overnight. The Proteinase K was then inactivated by heating at 95°C for 5 minutes. For genotyping using general PCR, 1 µL of the sample was added to the PCR mixture. For quantitative PCR (qPCR) for genotyping of XO mice, primers and probes were designed to amplify and detect the target DNA sequence from both the X chromosome and an autosome. The amount of amplification from the X chromosome was compared to the amount from the autosome to determine the genotype, specifically whether the sample (female) had one (XO) or two X (XX) chromosomes. The qPCR was performed in a CFX 96 Real-Time PCR machine.

Single cell RNA sequencing

Tissue samples were first dissected in PBS and then dissociated using 0.25% Trypsin/EDTA (Thermo Fisher, #25200056) at 37°C for approximately 20 minutes. Dissociation was stopped by

adding FBS (Thermo Fisher, #10439016) to a final concentration of 10%, and the resulting cell suspension was filtered through a 100 µm strainer (Fisher, #22-363-549) to remove any remaining undissociated structures. The cells were spun down by centrifugation using an Allegra X-14R Centrifuge (Beckman Coulter) at 300 × g for 3 minutes and then suspended in PBS containing 0.04% BSA. The samples were filtered through a 40 µm strainer (Fisher, #22-363-547) to remove doublets, followed by a second centrifugation using the Allegra X-14R Centrifuge (Beckman Coulter) at 300 × g for 5 minutes. The cells were then resuspended in an appropriate volume of PBS containing 0.04% BSA to achieve a cell concentration of 1000 cells/µl. Samples with a viability of over 90% were selected for subsequent sequencing. Libraries of the single cells were prepared using the Chromium Next GEM Single Cell 3' Reagent Kits v3.1(PN1000128) from 10X Genomics, with the goal of capturing 10,000 cells per sample. Sequencing was performed using the NextSeq 500 platform from Illumina according to 10X Genomics recommendations: paired-end, single index reads with Read 1 being 28 cycles, Index 1 being 8 cycles, and Read 2 being 91 cycles. Sequencing was performed to a depth of 50,000 reads per cell. The single cell sequencing datasets were initially processed using the Cell Ranger pipeline (v3.1.0 and v6.0.1) with default settings. Further analysis of the scRNA-seq data was performed using the Seurat package (v4.1.0). The count data were read and transformed into a Seurat object using the 'Read10X' and 'CreateSeuratObject' functions. The libraries (2 weeks, 3 weeks, 4 weeks, 5 weeks, and 6 weeks) were preprocessed with 'NormalizeData()', followed by 'FindVariableFeatures()', 'FindIntegrationAnchors()', and 'IntegrateData()' using default settings. The integrated object was further processed using 'ScaleData()', 'RunPCA(npcs = 50)', 'RunUMAP(dims = 1:30)', 'FindNeighbors(dims = 1:30)', 'FindClusters(resolution = 1.0)', and 'RunTSNE(dims = 1:30)' with other default settings to determine cell clusters. Further clustering

of granulosa cells and mesenchymal cells was performed using 'subset()', followed by the cell clustering methods mentioned above.

The electron microscope

Mice ovaries were excised and fixed in a solution of 2% PFA and 2.5% glutaraldehyde in 0.1 M PIPES buffer (MilliporeSigma, #P6757, pH 7.4) at 4°C overnight. The ovaries were then washed and treated with 50 mM glycine in 0.1 M PIPES buffer for 15 minutes, followed by washing with 0.1 M PIPES buffer. Tissue pieces were then postfixed with 1% osmium tetroxide and 1.5% potassium ferrocyanide in 0.1 M PIPES buffer for 60 minutes, washed with water, and stained *en bloc* with 1% (w/v) uranyl acetate for 60 minutes. The ovaries were then serially dehydrated using graded ethanol solutions: 30%, 50%, 75%, 85%, 95%, and 100% ethanol, followed by two exchanges of 100% acetone. After dehydration, the ovaries were infiltrated and embedded in EMbed 812 Epoxy resin (Electron Microscopy Sciences) according to the manufacturer's recommendations. Ultrathin sections at about 70 nm thick were cut on a Leica EM UC7 ultramicrotome and examined using a Hitachi HT7800 transmission electron microscope operated at 80 kV. Images were acquired with an AMT NanoSprint 12 camera.

Statistical analysis

The data are reported as means ± SD of biological replicates, and no statistical methods were used to determine the sample size. Differences between two groups were compared using a two-tailed Student's t-test. $P < 0.05$ was considered statistically significant.

Data availability

The scRNAseq data have been deposited at the NIH GEO database under accession number GSE268466.

ACKNOWLEDGEMENTS: We are grateful to Allison Pinder and Dr. Fredrick Tan for assisting with the genomic experiments and analyses. We thank Dr. Mamhud Siddiqi for his help with optical microscopy and image analyses. We thank Dr. Ru-Ching Hsia for expert electron microscopy. We thank the Carnegie Embryology support staff and Spradling lab members for comments on the study, especially Haolong Zhu for assistance with scRNA-seq data analysis.

Author contributions: Investigation: QY, Supervision and Funding: ACS, all other: QY and ACS.

Competing interests: None.

REFERENCES

Adolphi MC, Depince A, Wen M., Pan Q, Herpin A. (2023). Development of ovaries and sex change in fish: bringing potential into action. Sex Dev. 17, 84-98. doi: 10.1159/000526008.

Arnold AP. (2009). The organizational-activational hypothesis as the foundation for a unified theory of sexual differentiation of all mammalian tissues. Horm Behav. 5, 570-8. doi: 10.1016/j.yhbeh.2009.03.011.

Bell MR (2018). Comparing Postnatal Development of Gonadal Hormones and Associated Social Behaviors in Rats, Mice, and Humans. Endocrinology 159, 2596-2613. doi: 10.1210/en.2018-00220.

Bianco S, Bellefleur AM, Beaulieu É, Beauparlant CJ, Bertolin K, Droit A, Schoonjans K, Murphy BD & Gévry N (2019). The ovulatory signal precipitates LRH-1 transcriptional switching mediated by differential chromatin accessibility. *Cell Reports* **27** 2443.e4–2454.e4. (https://doi. org/10.1016/j.celrep.2019.07.088)

Boto P, Csuth TI, Szatmari (2018). I. RUNX3-Mediated Immune Cell Development and Maturation. Crit Rev Immunol. 38, 63-78. doi: 10.1615/CritRevImmunol.2018025488.

Browning HC (1973). The evolutionary history of the corpus luteum. Biology of Reproduction 8, 128-137.

Byskov, A.G.S. (1974). Cell kinetic studies of follicular atresia in the mouse ovary. J. Reprod. Fert. 37, 277-285.

Chang RJ. (2007). The reproductive phenotype in polycystic ovary syndrome. Nat Clin Pract Endocrinol Metab. 3, 688-95. doi: 10.1038/ncpendmet0637.

Cui J, Shen Y, Li R. (2013). Estrogen synthesis and signaling pathways during aging: from periphery to brain. Trends Mol Med. 19, 197-209. doi: 10.1016/j.molmed.2012.12.007.

DeFalco T, Capel B (2009). Gonad morphogenesis in vertebrates: divergent means to a convergent end. Annu. Rev. Cell Dev. Biol. 25, 457-482.

Devillers MM, François CM, Chester M, Corre R, Cluzet V, Giton F, Cohen-Tannoudji J, Guigon CJ. (2023). Androgen receptor signaling regulates follicular growth and steroidogenesis in interaction with gonadotropins in the ovary during mini-puberty in mice. Front Endocrinol (Lausanne). 14, 1130681. doi: 10.3389/fendo.2023.1130681.

Duggavathi R, Volle DH, Mataki C, Antal MC, Messaddeq N, Auwerx J, Murphy BD & Schoonjans K **(**2008). Liver receptor homolog 1 is essential for ovulation. *Genes and Development* **22** 1871–1876. (https://doi. org/10.1101/gad.472008)

Edson MA, Nagaraja AK, Matzuk MM. (2009). The mammalian ovary from genesis to revelation. Endocr Rev. 30, 624-712. doi: 10.1210/er.2009-0012.

Eppig JJ, Handel MA. (2012). Origins of granulosa cells clarified and complexified by waves. Biol Reprod 86, 34. doi: 10.1095/biolreprod.111.096651.

Erickson GF, Magoffin DA, Dyer CA, Hofeditz C. (1985). The ovarian androgen producing cells: a review of structure/function relationships. Endocr Rev. 6, 371-99. doi: 10.1210/edrv-6-3-371.

Faire M, Skillern A, Arora R, Nguyen DH, Wang J, Chamberlain C, German MS, Fung JC, Laird DJ. (2015). Follicle dynamics and global organization in the intact mouse ovary. Dev Biol. 403, 69-79. doi: 10.1016/j.ydbio.2015.04.006.

Feng Y, Cui P, Lu X, Hsueh B, Möller Billig F, Zarnescu Yanez L, Tomer R, Boerboom D, Carmeliet P, Deisseroth K, Hsueh AJ. (2017). CLARITY reveals dynamics of ovarian follicular architecture and vasculature in three-dimensions. Sci Rep. 7, 44810. doi: 10.1038/srep44810.

Fiorentino G, Parrilli A, Garagna S, Zuccotti M. (2020). Three-Dimensional Micro-Computed Tomography of the Adult Mouse Ovary. Front Cell Dev Biol. 8, 566152. doi: 10.3389/fcell.2020.566152.

François CM, Petit F, Giton F, Gougeon A, Ravel C, Magre S, Cohen-Tannoudji J, Guigon CJ. (2017). A novel action of follicle-stimulating hormone in the ovary promotes estradiol production without inducing excessive follicular growth before puberty. Sci Rep. 7, 46222. doi: 10.1038/srep46222.

Franks S, Hardy K (2010). Aberrant follicle development and anovulation in polycystic ovary syndrome. Annales d'Endocrinologie 71, 228–230.

Galas J, Slomczynska M, Knapczyk-Stwora K, Durlej M, Starowicz A, Tabarowski Z, Rutka K, Szoltys M. (2012). Steroid levels and the spatiotemporal expression of steroidogenic enzymes and androgen receptor in developing ovaries of immature rats. Acta Histochem 114, 207–216.

Gougeon A. (1996). Regulation of ovarian follicular development in primates: facts and hypotheses. Endocr Rev 17:121–155. doi: 10.1210/edrv-17-2-121. PMID: 8706629

Guzmán A, Hughes CHK, Murphy BD (2022). Liver receptor homolog 1 (LHR-1) regulates follicle vasculature during ovulation in mice. Reproduction 164, 283-289.

Guzmán A, Hernández-Coronado CG, Gutiérrez CG, Rosales-Torres AM. (2023). The vascular endothelial growth factor (VEGF) system as a key regulator of ovarian follicle angiogenesis and growth. Mol Reprod Dev. 90, 201-217. doi: 10.1002/mrd.23683.

Habara O, Logan CY, Kanai-Azuma M, Nusse R, Takase HM (2021). WNT signaling in pre-granulosa cells is required for ovarian folliculogenesis and female fertility. Development. 148, dev198846. doi: 10.1242/dev.198846.

Hirshfield AN. (1992). Heterogeneity of cell populations that contribute to the formation of primordial follicles in rats. Biol Reprod 47:466–472.

Hirshfield AN, DeSanti AM. (1995). Patterns of ovarian cell proliferation in rats during the embryonic period and the first three weeks postpartum. Biol Reprod 1995;53:1208 –1221.

Hsueh AJ, Billig H, Tsafriri A. (1994), Ovarian follicle atresia: a hormonally controlled apoptotic process. Endocr Rev. 15, 707-24. doi: 10.1210/edrv-15-6-707.

Jiménez R (2009).lOvarian organogenesis in mammals: mice cannot tell us everything. Sex Dev. 3, 2911-301.

Kelava I, Chiaradia I, Pellegrini L, Kalinka AT, Lancaster MA. (2022). Androgens increase excitatory neurogenic potential in human brain organoids. Nature 602, 112-116. doi: 10.1038/s41586-021-04330-4.

Khoa ND, Nakazawa M, Hasunuma T, Nakajima T, Nakamura H, Kobata T, Nishioka K. (2001). Potential role of HOXD9 in synoviocyte proliferation. Arthritis Rheum. 44, 1013-21. doi: 10.1002/1529-0131(200105)44:5<1013::AID-ANR180>3.0.CO;2-O.

Klein KO, Rosenfield RL, Santen RJ, Gawlik AM, Backeljauw PF, Gravholt CH, Sas TCJ, Mauras N (2018). Estrogen Replacement in Turner Syndrome: Literature Review and Practical Considerations. J Clin Endocrinol Metab. 103, 1790-1803. doi: 10.1210/jc.2017-02183.

Kumar TR, Wang Y, Lu N, Matzuk MM. (1997). Follicle stimulating hormone is required for ovarian follicle maturation but not male fertility. Nat Genet. 15, 201-4. doi: 10.1038/ng0297-201.

Lamas S, Carvalheira J, Gartner F, Amorim I. (2021). C57BL/6J mouse superovulation: schedule and age optimization to increase oocyte yield and reduce animal use. Zygote 29, 199-203. doi: 10.1017/S0967199420000714.

Li W, Germain RN, Gerner MY. (2017). Multiplex, quantitative cellular analysis in large tissue volumes with clearing-enhanced 3D microscopy (Ce3D). Proc Natl Acad Sci U S A. 114, E7321-E7330. doi: 10.1073/pnas.1708981114.

Liu C, Rodriguez K, Yao HHC. Mapping lineage progression of somatic progenitor cells in the mouse fetal testis. Development. 2016;143(20): 3700–3710.

McCartney, C. R. & Marshall, J. C. (2016). Polycystic ovary syndrome. N. Engl. J. Med. 375, 54–64.

McCarter J, Bartlett B, Dang T, Schedl T. (1997). Soma-germ cell interactions in Caenorhabditis elegans: multiple events of hermaphrodite germline development require the somatic sheath and spermathecal lineages. Dev Biol. 181, 121-43. doi: 10.1006/dbio.1996.8429. PMID: 9013925.

McGee EA, Hsueh AJ. (2000). Initial and cyclic recruitment of ovarian follicles. Endocr Rev 21:200–214. doi: 10.1210/edrv.21.2.0394.

McKey J, Anbarci DN, Bunce C, Ontiveros AE, Behringer RR, Capel B. (2022). Integration of mouse ovary morphogenesis with developmental dynamics of the oviduct, ovarian ligaments, and rete ovarii. Elife 11, e81088. doi: 10.7554/eLife.81088.

Meinsohn MC, Smith OE, Bertolin K, Murphy BD. (2019). The Orphan Nuclear Receptors Steroidogenic Factor-1 and Liver Receptor Homolog-1: Structure, Regulation, and Essential Roles in Mammalian Reproduction. Physiol Rev. 99, 1249-1279. doi: 10.1152/physrev.00019.2018.

Meinsohn MC, Hughes CHK, Estienne A, Saatcioglu HD, Pépin D, Duggavathi R, Murphy BD. (2021a). A role for orphan nuclear receptor liver receptor homolog-1 (LRH-1, NR5A2) in primordial follicle activation. Sci Rep. 11, 1079. doi: 10.1038/s41598-020-80178-4.

Meinsohn MC, Saatcioglu HD, Wei L, Li Y, Horn H, Chauvin M, Kano M, Nguyen NMP, Nagykery N, Kashiwagi A, Samore WR, Wang D, Oliva E, Gao G, Morris ME, Donahoe PK, Pepin D. (2021b). Single-Cell sequencing reveals suppressive transcriptional programs regulated by MIS/AMH in neonatal ovaries. PNAS 118, 20. doi: https://doi.org/10.1073/pnas.2100920118,

Miura K, Murata C, Harikae K, Suzuki H, Kanai-Azuma M, Kurohmaru M, Tsunekawa N, Kanai Y. (2017). Defects in the first wave of folliculogenesis in mouse XO ovaries. J Reprod Dev. 63, 333-338. doi: 10.1262/jrd.2017-033.

Miyabayashi K, Tokunaga K, Otake H, Baba T, Shima Y, Morohashi K. (2015). Heterogeneity of ovarian theca and interstitial gland cells in mice. PLoS One. 10, e0128352. doi: 10.1371/journal.pone.0128352.

Mork L, Maatouk DM, McMahon JA, Guo JJ, Zhang P, McMahon AP, Capel B (2012). Temporal differences in granulosa cell specification in the ovary reflect distinct follicle fates in mice. Biol Reprod. 86, 37. doi: 10.1095/biolreprod.111.095208.

Morris ME, Meinsohn MC, Chauvin M, Saatcioglu HD, Kashiwagi A, Sicher NA, Nguyen N, Yuan S, Stavely R, Hyun M, Donahoe PK, Sabatini BL, Pépin D. (2022). A single-cell atlas of the cycling murine ovary. Elife 11, e77239. doi: 10.7554/eLife.77239.

Nelson JF, Karelus K, Felicio LS, Johnson TE (1990). Genetic influences on the timing of puberty in mice. Biol Reprod. 42, 649-55. doi: 10.1095/biolreprod42.4.649.

Niu W, Spradling AC (2020). Two distinct pathways of pregranulosa cell differentiation support follicle formation in the mouse ovary. Proc Natl Acad Sci U S A. 117, 20015-20026. doi: 10.1073/pnas.2005570117.

Niu W, Spradling AC. (2022). Mouse oocytes develop in cysts with the help of nurse cells. Cell 185, 2576-2590. doi: 10.1016/j.cell.2022.05.001.

Poole DH, Ocón-Grove OM, Johnson AL. (2016). Anti-Müllerian hormone (AMH) receptor type II expression and AMH activity in bovine granulosa cells. Theriogenology 86, 1353-60. doi: 10.1016/j.theriogenology.2016.04.078.

Richards JS, Ren YA, Candelaria N, Adams JE, Rajkovic A. (2017). Ovarian Follicular Theca Cell Recruitment, Differentiation, and Impact on Fertility. Endocr Rev. 39, 1-20. doi: 10.1210/er.2017-00164.

Richards M, Nwadozi E, Pal S, Martinsson P, Kaakinen M, Gloger M, Sjöberg E, Koltowska K, Betsholtz C, Eklund L, Nordling S, Claesson-Welsh L (2022). Claudin5 protects the peripheral endothelial barrier in an organ and vessel-type-specific manner. Elife. 2022 11, e78517. doi: 10.7554/eLife.78517.

Rockey DC, Weymouth N, Shi Z. (2013). Smooth muscle α actin (Acta2) and myofibroblast function during hepatic wound healing. PLoS One. 8, e77166. doi: 10.1371/journal.pone.0077166.

Rotgers E, Jørgensen A, Yao HH-C (2018). At the crossroads of fate- somatic cell lineage specification in the fetal gonad. Endoc. Rev. 39, 739-759.

Simerly RB. (2002). Wired for reproduction: organization and development of sexually dimorphic circuits in the mammalian forebrain. Annu Rev Neurosci. 25, 507-36. doi: 10.1146/annurev.neuro.25.112701.142745. .

Sisk CL, Zehr JL. (2005). Pubertal hormones organize the adolescent brain and behavior. Front Neuroendocrinol. 26, 163-74. doi: 10.1016/j.yfrne.2005.10.003.

Sjöberg E, Meyrath M, Milde L, Herrera M, Lövrot J, Hägerstrand D, Frings O, Bartish M, Rolny C, Sonnhammer E, Chevigné A, Augsten M, Östman A. (2019). A Novel ACKR2-Dependent Role of Fibroblast-Derived CXCL14 in Epithelial-to-Mesenchymal Transition and Metastasis of Breast Cancer. Clin Cancer Res. 25, 3702-3717. doi: 10.1158/1078-0432.CCR-18-1294.

Sun C, Zhang K, Ni C, Wan J, Duan X, Lou X, Yao X, Li X, Wang M, Gu Z, Yang P, Li Z, Qin Z. (2023). Transgelin promotes lung cancer progression via activation of cancer-associated fibroblasts with enhanced IL-6 release. Oncogenesis 12, 18. doi: 10.1038/s41389-023-00463-5.

Templin JS, Wyrosdic JC, David CD, Wyrosdic BN, Lapp HE, Bala A, Bartlett A, Khan Z, Rokicki A, Park JH. (2019). Peripubertal gonadal steroids are necessary for steroid-independent male sexual behavior in castrated B6D2F1 male mice. Horm Behav. 113, 38-46. doi: 10.1016/j.yhbeh.2019.04.013.

Trova S, Bovetti S, Bonzano S, De Marchis S, Peretto P. (2021). Sex Steroids and the Shaping of the Peripubertal Brain: The Sexual-Dimorphic Set-Up of Adult Neurogenesis. Int J Mol Sci. 22, 7984. doi: 10.3390/ijms22157984.

Viuff MH, Just J, Brun S, Dam TV, Hansen M, Melgaard L, Hougaard DM, Lappe M, Gravholt CH (2022). Women With Turner Syndrome Are Both Estrogen and Androgen Deficient: The Impact of Hormone Replacement Therapy. J Clin Endocrinol Metab. 107, 1983-1993. doi: 10.1210/clinem/dgac167.

Walters KA, Rodriguez Paris V, Aflatounian A, Handelsman DJ (2019). Androgens and ovarian function: translation from basic discovery research to clinical impact. J Endocrinol. 242, R23-R50. doi: 10.1530/JOE-19-0096.

Wang Y, Pan L, Moens CB, Appel B. (2014). Notch3 establishes brain vascular integrity by regulating pericyte number. Development 141, 307-17. doi: 10.1242/dev.096107.

Wang Y, Zhao Y, Chen S, Chen X, Zhang Y, Chen H, Liao Y, Zhang J, Wu D, Chu H, Huang H, Wu C, Huang S, Xu H, Jia B, Liu J, Feng B, Li Z, Qin D, Pei D, Cai J. (2022). Single cell atlas of developing mouse dental germs reveals populations of CD24+ and Plac8+ odontogenic cells. Sci Bull (Beijing) 67, 1154-1169. doi: 10.1016/j.scib.2022.03.012.

Xie T, Wang Y, Deng N, Huang G, Taghavifar F, Geng Y, Liu N, Kulur V, Yao C, Chen P, Liu Z, Stripp B, Tang J, Liang J, Noble PW, Jiang D. (2018). Single-Cell Deconvolution of Fibroblast Heterogeneity in Mouse Pulmonary Fibrosis. Cell Rep. 22, 3625-3640. doi: 10.1016/j.celrep.2018.03.010.

Yoest KE, Henry MG, Velisek HA, Veenema AH. (2023). Development of social recognition ability in female rats: Effect of pubertal ovarian hormones. Horm Behav. 151, 105347. doi: 10.1016/j.yhbeh.2023.105347.

Young JM, McNeilly AS (2010). Theca: the forgotten cell of the ovarian follicle. Reproduction. 140, 489-504. doi: 10.1530/REP-10-0094.

Zhang J, Lu S, Lu T, Han D, Zhang K, Gan L, Wu X, Li Y, Zhao X, Li Z, Shen Y, Hu S, Yang F, Wen W, Qin W. (2023). Single-cell analysis reveals the COL11A1+ fibroblasts are

cancer-specific fibroblasts that promote tumor progression. Front Pharmacol. 14, 1121586. doi: 10.3389/fphar.2023.1121586.

Zheng W, Zhang H, Gorre N, Risal S, Shen Y, Liu K (2014a). Two classes of ovarian primordial follicles exhibit distinct developmental dynamics and physiological functions. Hum Mol Genet. 23, 920-28. doi: 10.1093/hmg/ddt486.

Zheng W, Zhang H, Liu K (2014b). The two classes of primordial follicles in the mouse ovary: their development, physiological functions and implications for future research. Mol Hum Reprod. 20, 286-292. doi: 10.1093/molehr/gau007.

Zhou J, Jiang X, Wu H, Zhang L, Chen M, Chen M, Shen Z, Guo X, Wang H, Gao F. Dissecting the fate of Foxl2-expressing cells in fetal ovary using lineage tracing and single-cell transcriptomics. Cell Discov. 2022 Dec 27;8(1):139. doi: 10.1038/s41421-022-00492-1. PMID: 36575161; PMCID: PMC9794781.

Zhou Y, Zhu W, Guo Z, Zhao Y, Song Z, Xiao J (2007). Effects of maternal nuclear genome on the timing of puberty in mice offspring. J Endocrinol. 193, 405-12. doi: 10.1677/joe.1.07049.

Zhou Y, Zhou B, Pache L, Chang M, Khodabakhshi AH, Tanaseichuk O, Benner C, Chanda SK. (2019. Metascape provides a biologist-oriented resource for the analysis of systems-level datasets. Nat Commun. 10, 1523. doi: 10.1038/s41467-019-09234-6.

Zuckerman-Levin N, Frolova-Bishara T, Militianu D, Levin M, Aharon-Peretz J, Hochberg Z (2009). Androgen replacement therapy in Turner syndrome: a pilot study. J Clin Endocrinol Metab. 94, 4820-7. doi: 10.1210/jc.2009-0514.

FIGURE LEGENDS

Figure 1. Wave 1 follicles are remodeled prior to peri-puberty.

(A). Schematic diagrams of fetal ovaries at indicated stages (above: E =embryonic day; P = postnatal day). Wave 1 follicles in the ovarian medulla (below dashed line) retain bipotential pregranulosa cells (BPGs) and develop without delay; epithelial pregranulosa cells (EPGs) replace BPGs on follicles in the cortex which become quiescent primordial follicles (wave 2).

(B) Postnatal follicular developmental timeline: wave 1 antral follicles: 2 weeks (Figure S1A-C); juvenile sexual development (peri-puberty): 4-5 weeks; puberty and ovulation: 7-8 weeks.

(C) Total follicles or wave 1 follicles (D) in P5 or P10 ovaries (see Figure S1E-F)

(E) Wave 1 ovarian volume vs age (mean +/- SD (bars); N=10)

(F) Wave 1 follicle remodeling (%) indicated by oocyte loss vs age (mean +/- SD (bars); N=3-4).

Figure 2. Wave 1 follicles lose granulosa cells during remodeling.

(A) Schematic diagram showing activation of *Foxl2*-CreER^{T2} expression initiated by Tamoxifen (TAM) injection leading to excision of a stop cassette and EYFP expression (see Methods).

(B) Efficient EYFP labeling of granulosa cells in wave 1 medullar follicles of a 2-week ovary following TAM injection at E16.5 as shown in (A). Note virtual absence of labeling in cortical wave 2 follicles (right).

(C-D) Views of whole ovaries labeled as in A, and imaged at 2 week (C) or 5 week (D) and processed using Imaris to mark location of wave 1 follicles (balls).

(E) Wave 1 follicle numbers from Imaris analysis of (C-D).

(F) Section from a 5 week ovary from (D) reveals ongoing remodeling of wave 1 follicles. Follicles near the medullar core are small (arrowheads), with few remaining EYFP-labeled granulosa cells, such as the follicle boxed in "1" (F'). A normal antral follicle "2" (F") with an oocyte contains many EYFP labeled granulosa cells. At right, the average number of EYFP-labeled GCs in medullar follicles prior to remodeling at 3 weeks is compared to the average number in remodeled medullar follicles at 5 weeks. Each point represents one analyzed follicle. **** $p<0.0001$.

(G) A 6 week ovary after TAM injection at 5 week. A few central GCs in remodeled wave 1 follicles near the center of the image are labeled, showing they still express *Foxl2* at 5 weeks.

<u>Figure 3. Follicles remodel to form an interconnected stromal network rich in thecal secretory cells.</u>

(A) Schematic diagraming showing lineage labeling of *Cyp17a1*-epxressing thecal cells and interstitial gland cells, and possibly other cells using *Cyp17a1*-iCre; CAG-tdTomato.

(B) 2 week ovary showing tdTomato-labeling of thecal cells sheathing follicles (arrowhead) and putative interstitial gland cells between follicles (rectangle).

(C) 3D reconstruction of follicles from with surrounding labeled thecal cells: Oocytes (green, DDX4), *Cyp17a1*-expressing cells (red). Scale bar, 20 µm.

(D-E) Whole mount staining of 2 week and 5 week ovary labeled, showing dramatic increase in labeled thecal, interstitial and possibly other *Cyp17a1*-lineage marked cells in the ovarian medulla.

(F-G) Oil red O staining (red color) reveals a significant increase in lipid droplet storage in ovarian medullar cells from 2 week (F) to 5 week (G) ovaries. Scale bar, 100 µm.

(H). Immunofluorescence staining of HSD3B1 and PLIN1 at 5 weeks shows that genes required for steroidogenesis and lipid droplet storage are highly expressed in medullar cells. Scale bar, 50 µm.

(I) Electron microscopy of remodeled thecal network showing cells with abundant lipid droplets (LD) and characteristic mitochondria (mt) (boxed region magnified in right panel). Scale bar, 10 µm.

(J) 3D reconstruction of an entire 5week ovary labeled by tdTomato expression activated by *Cyp17a1*-iCre. Scale bar, 100 µm.

Figure 4. Single-cell RNA sequencing of 2 wk-6 wk ovaries

(A) UMAP plot of ovaries from 2 weeks to 6 weeks, showing 31 initial clusters (c0-c30). (A') the cell type groups indicated by colored regions as labeled and their relationship to the numbered initial clusters as shown in A.

(B) UMAP plot of re-clustered granulosa cells from A showing 18 clusters (gc0-gc17) (B') the deduced ovarian follicle developmental stages labeled and indicated by colored regions and their relationship to the numbered clusters (numbers) shown in B.

(C) UMAP plot of re-clustered thecal, stromal and smooth muscle cells from A showing 21 clusters (gc0-gc20). (C') the deduced mesodermal cell subgroups labeled and indicated by colored regions and their relationship to the numbered clusters (numbers) shown in C.

(D) Diagram of steroidogenic genes in theca and granulosa cells giving rise to androgens such as testosterone and androstenedione, and their conversion in granulosa to estrogen. The diagram

illustrates the expression of steroidogenic genes in theca and granulosa cells, which contribute to the synthesis of androgens, such as testosterone and androstenedione, and their subsequent conversion to estrogen within granulosa cells. The estimated numbers of steroidogenic theca cells expressing three key genes in the steroidogenesis pathway—*Cyp11a1*, *Hsd3b1*, and *Cyp17a1*—are shown, and those expressing four genes in the pathway (the previous three plus Star). Additionally, the estimated numbers of granulosa cells expressing *Hsd3b1*, *Hsd17b1*, and *Cyp19a1* are presented.

(E) The estimated number of granulosa cells in follicles of the indicated developmental subclasses: primordial, primary, secondary, antral, remodeling, mitotic cycling.

Figure 5. Model of wave 1 follicle development and function.

(A) Current model of follicle waves in juvenile mice (revised from 1A). Wave 1 follicles remodel to expand androgen-producing theca/interstitial cells during peri-puberty. There are gradients between the medulla and cortex that facilitate the sequential activation of primordial follicles, continuing at least early into adult period.

(B) A diagram showing the deduced and proposed pathway of wave 1 follicle remodeling beginning at about 3 weeks. These steps are 1) oocyte (blue) loss; 2) loss of most granulosa cells (maroon); 3) expansion of steroidogenic, increase and interconnection of angiogenic and fibroblastic thecal cells (tan rectangles); 4) androgen biosynthesis and release contributing to normal juvenile development during peri-puberty, and support of new normal follicles (5 weeks).

SUPPLEMENTARY MATERIALS

Supplementary Tables

Table S1. Summary of whole mount C57BL/6J ovary analyses.

Postnatal age	Total follicles/ ovary *	Antral follicles*	Wave 1 follicles *	Reference files	Ovaries analyzed
P5-7	3822 +/- 838	0	278 +/- 17	S1.mp4; S2.mp4	4
P10-14	3304 +/- 926	0	293 +/- 36	S3.mp4; S4.mp4	3
3 wk	3089 +/- 669	23 +/- 2	ND	S5.mp4 S6.mp4	3
4 wk	ND	35 +/- 2	ND	S7.mp4 S8.mp4	4
5 wk	ND	24 +/- 4	ND	S9.mp4 S10.mp4	5

* numbers are mean and standard deviation

All samples were subjected to whole mount staining using a DDX4 antibody and DAPI. Oocytes or follicles were manually counted by identifying DDX4-positive oocytes surrounded by granulosa cells, until reaching the later antral follicle stage, where DDX4 expression ceases. All ovaries at each stage were collected from at least two litters. Follicles with multiple layers of granulosa cells and a visible antrum were categorized as antral follicles. At P5-7 and P10-14, follicles with oocytes greater than 20 µm in diameter (mostly located in the medulla) and cuboidal granulosa cells were classified as wave one follicles. All videos were exported from Imaris.

SUPPLEMENTARY METHOD DETAILS

MATERIALS

Antibodies

Name	Source	Identifier	Dilution
Anti-EGFP (Chicken)	Aves labs	GFP-1020	1:300
Anti-DDX4 (Rabbit)	Abcam	ab13840	1:300
Anti-MSY2 (Mouse)	Abcam	sc-393840	1:100
Anti-tdTomato (Goat)	Origene Tech	AB8181-200	1:300
Anti-HSD3B1 (Mouse)	Santa Cruz	sc-515120	1:100
Anti-CYP17A1 (Rabbit)	Cell Signaling Technology	94004T	1:100
Anti-PLIN1 (Rabbit)	abcam	ab3526	1:100
DAPI	Sigma	D9542-10mg	0.5ug/ml
Alexa Fluor® 488 AffiniPure™ Donkey Anti-Chicken IgY (IgG) (H+L)	Jacksonimmuno	703-545-155	1:300
Alexa Fluor® 594 AffiniPure™ Donkey Anti-Goat IgG (H+L)	Jacksonimmuno	705-585-147	1:300
Alexa Fluor 488 donkey anti-mouse lgG	invitrogen	A21202	1:300
Alexa Fluor 568 donkey anti-mouse lgG	invitrogen	A10037	1:300
Alexa Fluor 488 donkey anti-rabbit lgG	invitrogen	A21206	1:300
Alexa Fluor 568 donkey anti-rabbit lgG	invitrogen	A10042	1:300
Alexa Fluor 647 donkey anti-rabbit lgG	invitrogen	A31573	1:300

Primers

Name	Forward (5'-3')	Reverse (5'-3')	Size	Chromosome	Note
XO-qPCR-Tg	GACTAGGTTCATAGGCACTGG	CCGCCAAAACTCCTTCTCTAC	123 bp	X	Genotyping for XO mice
XO-qPCR-Tg-Probe	[5HEX]CCCCAGATGGTACCCACAGAACTTG			X	
XO-qPCR-IPC	CACGTGGGCTCCAGCATT	TCACCAGTCATTTCTGCCTTTG	74 bp	12	
XO-qPCR-IPC-Probe	[Cy5]CCAATGGTCGGGCACTGCTCAA			12	
Foxl2-Mutant	AGAGAAGAGAGTGAGAGCCG	GTCCAGCTCGACCAGGATGG	221 bp	9	Genotyping for *Foxl2*-CreER^{T2}
Foxl2-WT	AGAGAAGAGAGTGAGAGCCG	GAGCGCCACGTACGAGTACG	335 bp	9	
Cyp17a1-Tg	GCTGTAGCTTCTCCACTCCAC	CAGGTTTTGGTGCACAGTCA	120 bp		Genotyping for *Cyp17a1*-iCre
Cyp17a1-IPC	AGTGGCCTCTTCCAGAAATG	TGCGACTGTGTCTGATTTCC	521 bp		

SUPPLEMENTARY FIGURE LEGENDS

Fig. S1. Wave 1 follicle development in the early juvenile ovary.

(A-D) Wave 1 follicles stained for DDX4 (green) at P5, P7, P14 (2 weeks) and P21 (3 weeks). Based on cell morphology (arrow) theca cells are already forming at P5 (A). The follicles go through to late primary at P7 with more granulosa cells in one layer (B), to secondary follicle at P14 with several layers of granulosa cells (C) and to antral follicles at P21 with the oocyte forming non-surrounded nucleolus (D).

(E-F') Quantification of wave 1 (E-F) and total (E'-F') follicles throughout the ovary using Ce3D clearing solution and Imaris software (gray balls). The follicles with oocytes >20 μm in diameter (located mostly in medulla) are considered to be wave 1 follicles; all DDX4 positive cells counted manually were used to define total follicles.

(G-G') Whole mount staining and 3D reconstruction of ovary at P14. A surface model generated using Imaris software defines the oocyte boundaries, excluding the nucleus.

Fig. S2. Wave 1 follicles begin to remodel by 3 wk.

(A) C57BL/6J ovaries stained for DDX4 (green) and DAPI showing extensive remodeling (formerly termed "atresia") of wave 1 follicles (arrowheads). Some normal developing follicles are present(arrows) that probably represent follicles activated after wave 1. Left (4 weeks): Oocyte become distorted, and granulosa cells are reduced in number and no longer form well-organized layers. Right (5 weeks): Boundaries between former follicles become indistinct and holes left by the degenerated nuclei shrink in size but are still visible.

(B) Electron microscopy of wave 1 follicles. In a normal follicle, the oocyte is closely intact with the zona pellucida (ZP) and even granulosa cells through microvilli. In a remodeling

intermediate follicle, the cytoplasm of the oocyte shrinks, as indicated by the space between the oocyte and ZP, and the absence of microvilli on the ZP. In a fully remodeling follicle, the oocyte disappears, while the ZP persists; the thecal cells and related interstitial gland cells further accumulate lipid droplets. Oo: Oocyte; ZP: Zona pellucida; LD: Lipid droplet; mt: Mitochondria. (C) DAPI-stained DBA/2J ovaries showing wave 1 follicle remodeling (arrowheads) and normal developing follicles (arrows). Left (3 weeks): Early remodeling follicles are found in the central medulla. Right (7 weeks): wave 1 derivatives that still retain holes remain visible (arrowheads) along with normal follicles (arrows) and corpus lutei (asterisks).

Fig. S3. Lineage tracing wave 1 granulosa cells

(A-D) Lineage labeling using *Foxl2*-CreER^{T2} and CAG-tdTomato. Tamoxifen was administrated at E16.5. (B) Control experiment to rule out EGFP expression from the *Foxl2*-EGFP-CreR^{T2} construct contributes to apparent EYFP granulosa cell labeling in Figure 2 and Figure S3D-J). Note that EGFP expression from *Foxl2*-EGFP-CreR^{T2} is very low, and its expression pattern (cytoplasmic only, differs from the strong cytoplasm and nuclear expression of EYFP after stop sequence removal). At 2 weeks, many small primordial follicles located near the cortex-medulla border are partially labeled (examples shown in C) in addition to large wave 1 follicles in the medulla. By 5 weeks, wave 1 follicles have remodeled, while large follicles contain granulosa cells mosaic for Tomato expression, fully recapitulating the previous results with EYFP. These intact large follicles, most likely derived from wave 2 progenitors. Arrowhead: remodeled wave 1 follicle; arrow: large follicle with mosaic tdTomato expression. Primary follicle (enlarged in D), showing that EGFP expression from *Foxl2*-EGFP-CreR^{T2} is confined to the cell cytoplasm, unlike the expression observed in previous experiments using activated EYFP expression.

(E-I) Lineage labeling using *Foxl2*-CreER^{T2} and CAG-EYFP. At 2 weeks, one or more granulosa cells (E) in some primordial follicles are labeled by EYFP (enlarged in "1", "2", "3"). (F) Counts showed that 7% (421+/-74) of 5,843+/-1256 total primordial follicles contained EYFP-labeled granulosa cells (E, see also Fig. 1D). (G) About 80% of remodeled follicles still contain some EYFP-labeled granulosa cells at 5 weeks, consistent with their wave 1 origin. Dashed line: contour of follicle; arrowheads: EYFP-positive granulosa cells. Labeled PFs: Labeled primordial follicles.

(H) About 70% of secondary follicles in 5 week ovaries, also contain EYFP-labeled granulosa cells suggesting that they also derive from labeled primordial follicles at 2 weeks.

(I) After lineage labeling ovarian cells at E16.5 (Figure 2E), >90% of wave 1 follicles have EYFP-positive granulosa cells at 2weeks. At 5wk > 70% of normal antral follicles (Total 37) contain EYFP-positive granulosa cells, even though >80% of wave 1 follicles have lost oocytes and remodeled (Figure 1F).

(J) Lineage labeling using *Foxl2*-CreER^{T2} and CAG-EYFP. Tamoxifen was administrated at E14.5. At 2 weeks, one or more granulosa cells in some primordial follicles are labeled by EYFP (enlarged in "1").

<u>Fig. S4. Expansion of theca cells and its related cells - interstitial gland population.</u>

(A) Immunofluorescence staining of CYP19A1 in the ovary at 3 weeks and 5 weeks. Significant increase of theca cells and interstitial gland is observed at stroma from 3 weeks to 5 weeks.

(B-C) Immunofluorescence staining of *Cyp17a1* lineage-traced ovary at 2 weeks. Initially, expression was observed in theca cells and associated cells that appear to be interstitial gland cells (arrows). In addition, a few granulosa cells were labeled (arrowheads), as reported before (Bridges et al., 2008).

(D) *Cyp17a1* lineage-traced ovary at 4 weeks and 7 weeks. A significant increase in the number of labeled theca cells and interstitial gland cells is observed at 7 weeks compared to 4 weeks. In this staining, the signals from labeled theca cells and interstitial gland cells are much brighter than those from granulosa cells. This is likely because the tdTomato antibody has more difficulty penetrating the follicle to reach granulosa cells compared to the theca cells and interstitial gland cells. (E) Structurally, steroidogenic theca cells closely resemble interstitial cells. In the image, red lines are used to distinguish zones enriched in interstitial cells (1), theca cells (2), and granulosa cells (3). The rectangle labeled "1" indicates interstitial cells, while the rectangle labeled "2" represents steroidogenic theca cells, and the rectangle labeled "3" indicates granulosa cells. nu: Nucleus. LD: Lipid droplet; mt: Mitochondria.

Fig. S5. Analysis of single-cell RNA sequencing

(A) The ovarian cells from 2 to 6 weeks contribute to almost every cluster in the UMAP plot.

(B) Summary of marker gene expression in cell clusters, including granulosa cells, stromal cells, theca cells, epithelial cells, smooth muscle cells, endothelial cells, pericytes, hematopoietic cells, TBD (to be determined) cells, and cells with low UMI or higher mitochondrial content.

(C) The marker gene expression for granulosa cells from different stages of follicles, including primordial follicle, primary follicle, secondary follicle, antral follicle, remodeling follicle, and cells in mitotic cycles.

(D) The marker gene expression for the reanalysis of mesenchymal cells, including stromal theca cells expressing *Cyp17a1*, *Tagln*+ fibroblasts, *Col14a1*+ fibroblasts, *Cd24a*+ fibroblasts, *Cxcl12*+ fibroblasts, *Hox9*+ fibroblasts, *Col11a1*+ fibroblasts and mitotic cells expressing *Mki67*.

Fig. S6. Hormone receptor expression and XO mouse line.

(A) Androgen receptor is expressed in almost all cell types, while estrogen receptor 1 (*Esr1*) is expressed in theca cells, epithelial cells, and smooth muscle cells and Estrogen receptor 2 (*Esr2*) is expressed in granulosa cells and some TBD (To be determined) cells. No follicle-stimulating hormone receptor (Fshr) is expressed, and luteinizing hormone/choriogonadotropin receptor (*Lhcgr*) is expressed in theca cells.

(B) The total number of follicles in XO mice at 1 week is significantly less than in control XX mice.

(C) Activated follicles (normally wave 1 follicles, but not so in XO mice) in XO mice are much less than activated follicles in XX mice at 1 week, but are replenished by some wave 2 or wave 1.5 follicles by 2 weeks, as there is no statistical difference between XO and XX at 2 weeks.

Fig. 1

A

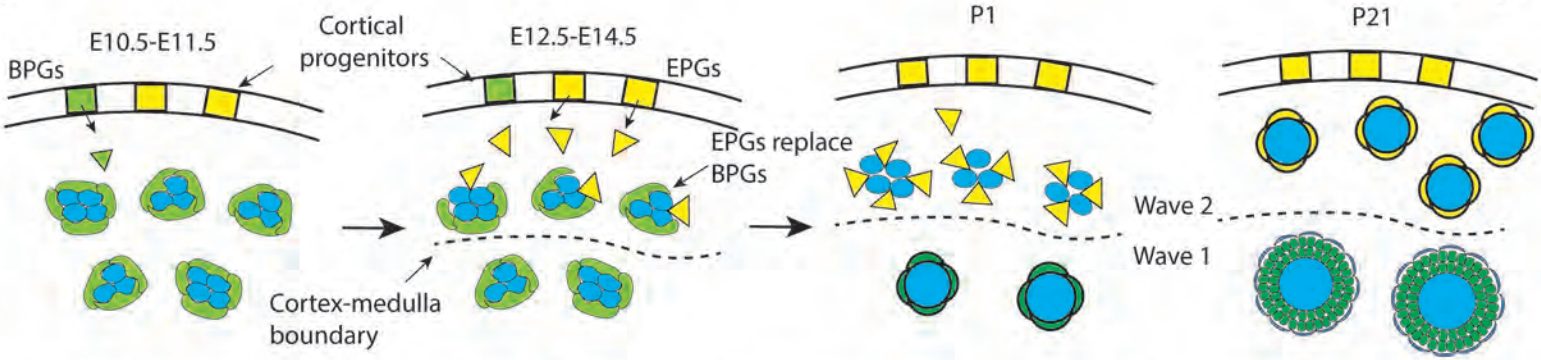
E10.5-E11.5
BPGs
Cortical progenitors
E12.5-E14.5
EPGs
EPGs replace BPGs
P1
P21
Wave 2
Wave 1
Cortex-medulla boundary

B

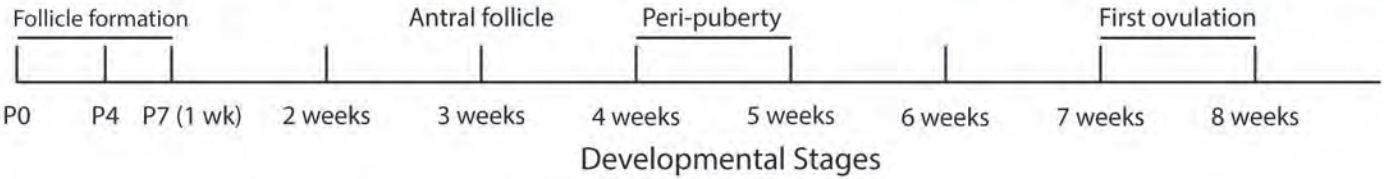
Follicle formation
Antral follicle
Peri-puberty
First ovulation
P0
P4
P7 (1 wk)
2 weeks
3 weeks
4 weeks
5 weeks
6 weeks
7 weeks
8 weeks
Developmental Stages

C

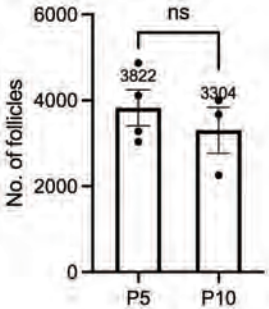
Total
ns
3822
3304
No. of follicles
6000
4000
2000
0
P5
P10

D

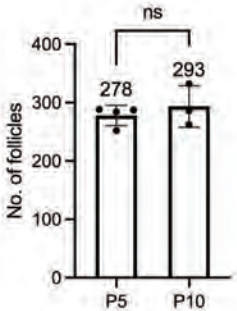
Wave 1
ns
278
293
No. of follicles
400
300
200
100
0
P5
P10

E

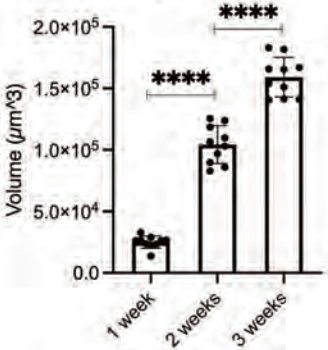
Oocyte volume
****
****
Volume (μm^3)
2.0×10^5
1.5×10^5
1.0×10^5
5.0×10^4
0.0
1 week
2 weeks
3 weeks

F

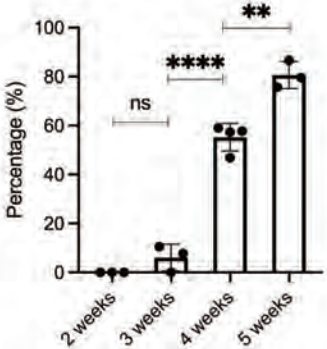
Wave 1 oocyte loss
ns
****
**
Percentage (%)
100
80
60
40
20
0
2 weeks
3 weeks
4 weeks
5 weeks

Fig. 2

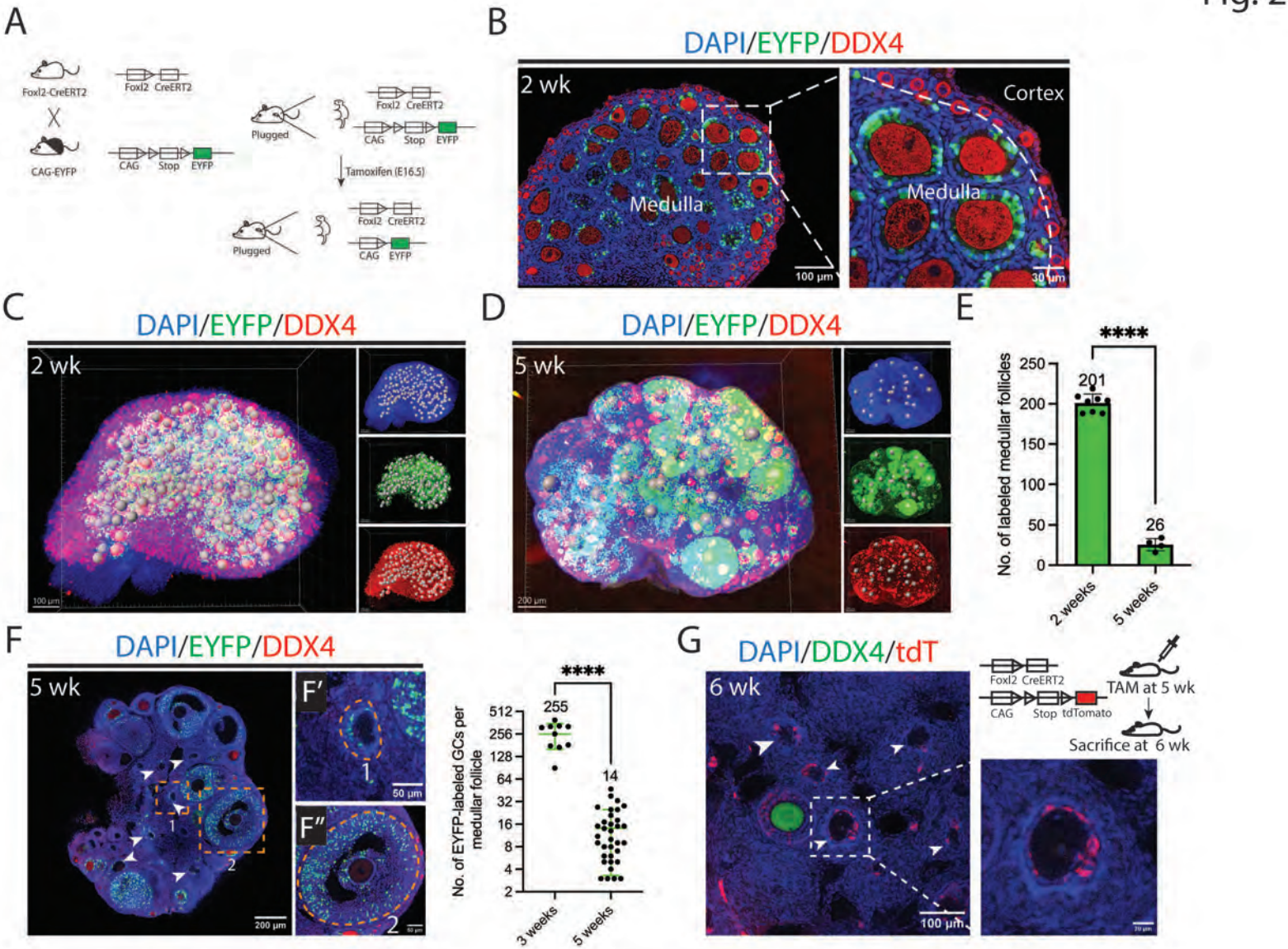
A
Foxl2-CreERT2
Foxl2 CreERT2
CAG-EYFP
CAG Stop EYFP
Plugged
Foxl2 CreERT2
CAG Stop EYFP
Tamoxifen (E16.5)
Plugged
Foxl2 CreERT2
CAG EYFP
B
DAPI/EYFP/DDX4
2 wk
Medulla
100 µm
Cortex
Medulla
30 µm
C
DAPI/EYFP/DDX4
2 wk
100 µm
D
DAPI/EYFP/DDX4
5 wk
200 µm
E
****
No. of labeled medullar follicles
250
200
150
100
50
0
201
26
2 weeks
5 weeks
F
DAPI/EYFP/DDX4
5 wk
1
2
200 µm
F′
1
50 µm
F″
2
****
No. of EYFP-labeled GCs per medullar follicle
512
256
128
64
32
16
8
4
2
255
14
3 weeks
5 weeks
G
DAPI/DDX4/tdT
6 wk
100 µm
Foxl2 CreERT2
CAG Stop tdTomato
TAM at 5 wk
Sacrifice at 6 wk

Fig. 3

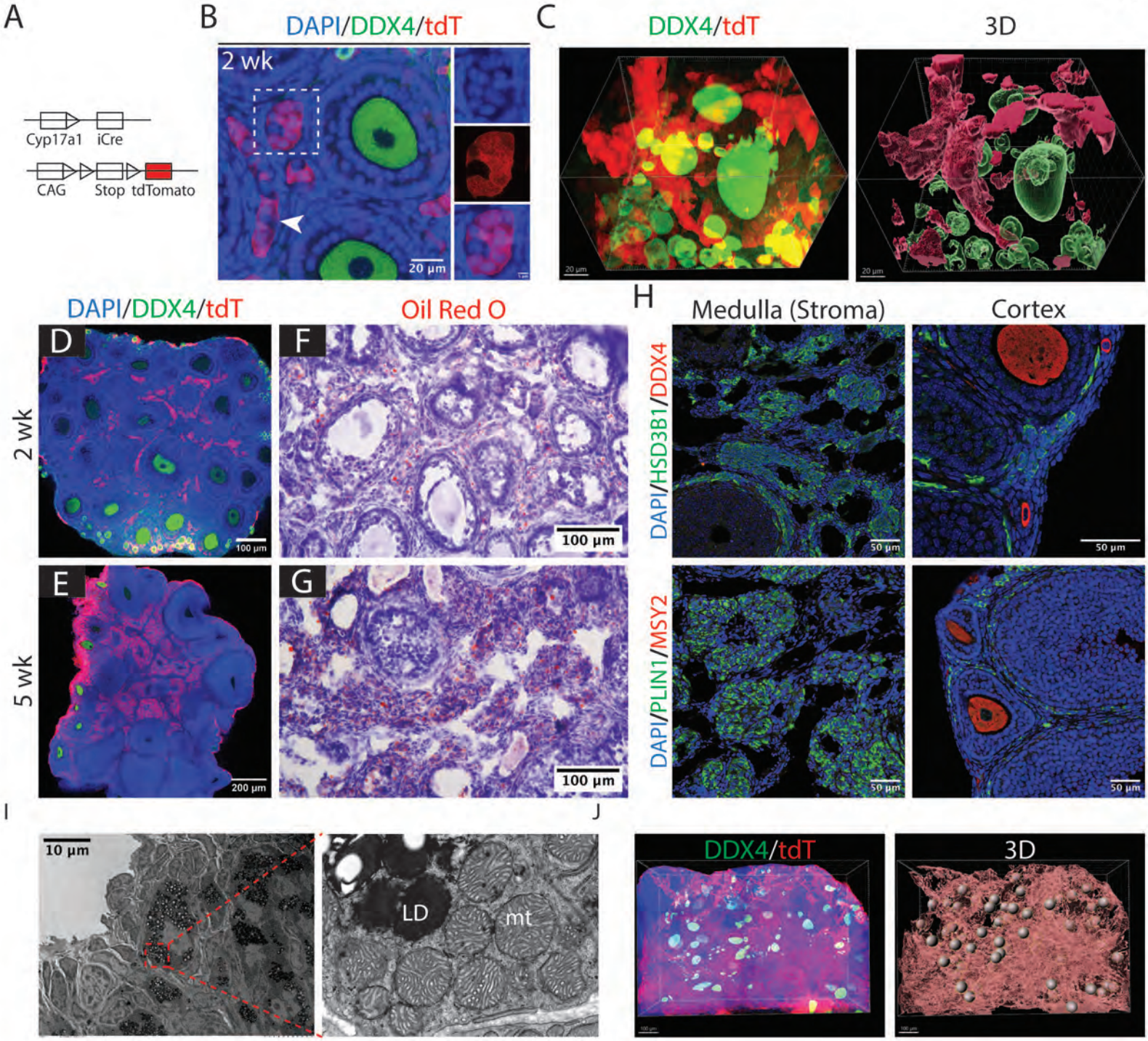
A
Cyp17a1
iCre
CAG
Stop
tdTomato
B
DAPI/DDX4/tdT
2 wk
20 µm
C
DDX4/tdT
3D
20 µm
DAPI/DDX4/tdT
Oil Red O
D
F
2 wk
100 µm
100 µm
E
G
5 wk
200 µm
100 µm
H
Medulla (Stroma)
Cortex
DAPI/HSD3B1/DDX4
DAPI/PLIN1/MSY2
50 µm
50 µm
50 µm
50 µm
I
J
10 µm
LD
mt
DDX4/tdT
3D

Fig. 4

A

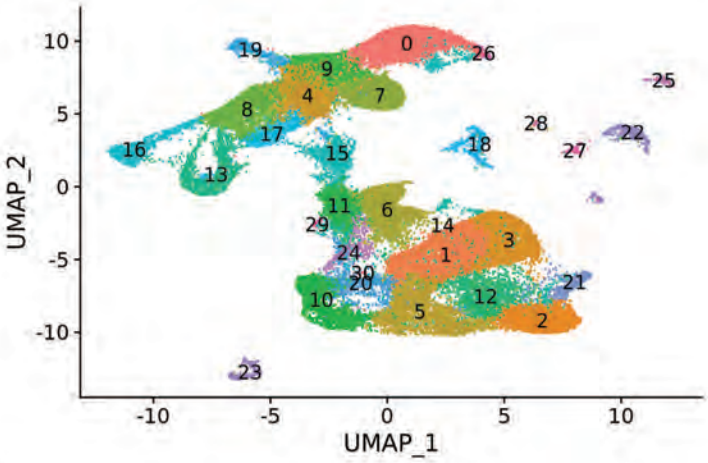

A′

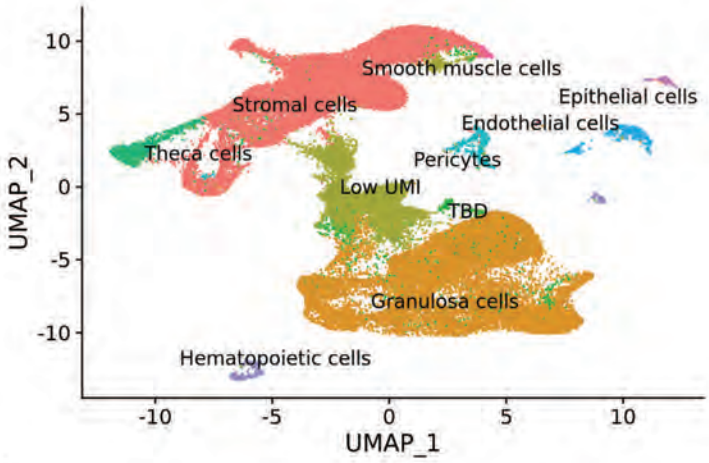

B

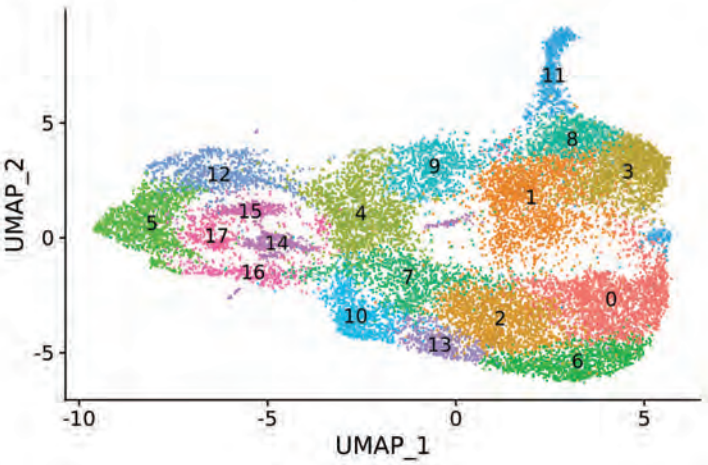

B′

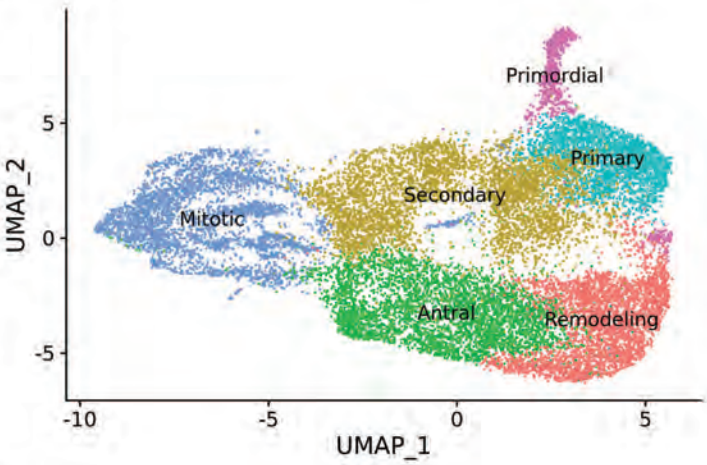

C

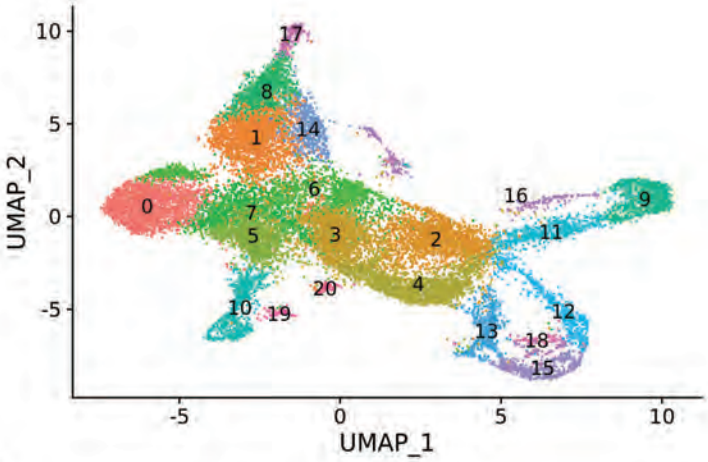

C′

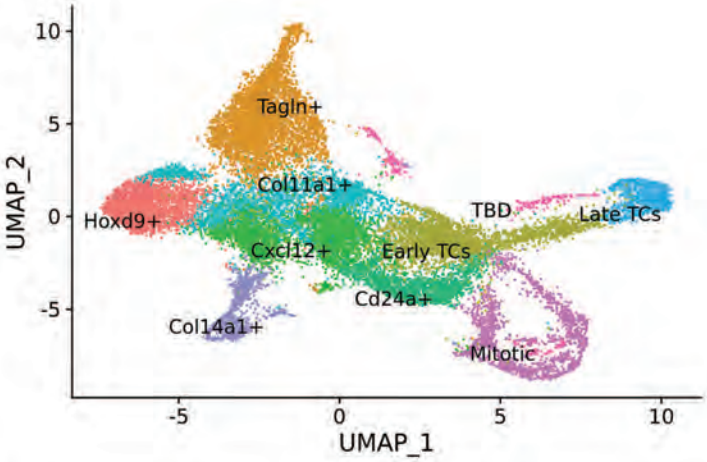

D

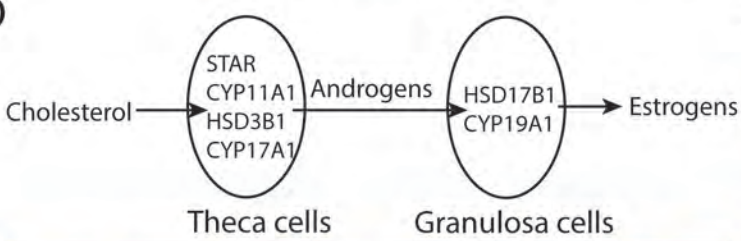

		2 wk (9471)	3 wk (9253)	4 wk (11077)	5 wk (7779)	6 wk (10583)
Theca cells	Cyp11a1 &Hsd3b1 &Cyp17a1	96	75	147	633	89
	Cyp11a1 &Hsd3b1 &Cyp17a1 &Star	41 (42.7%)	32 (42.7%)	72 (49.0%)	526 (83.1%)	29 (32.6%)
Granulosa cells	Hsd3b1 &Hsd17b1 &Cyp19a1	247	202	68	238	626

E

	2 wk	3 wk	4 wk	5 wk	6 wk
Primordial	316	206	124	81	81
Primary	794	742	392	230	365
Secondary	1086	1131	896	442	760
Antral	356	587	1416	590	1050
Remodeling	77	138	1348	766	910
Mitotic cycling	478	647	1072	620	749

Fig. 5

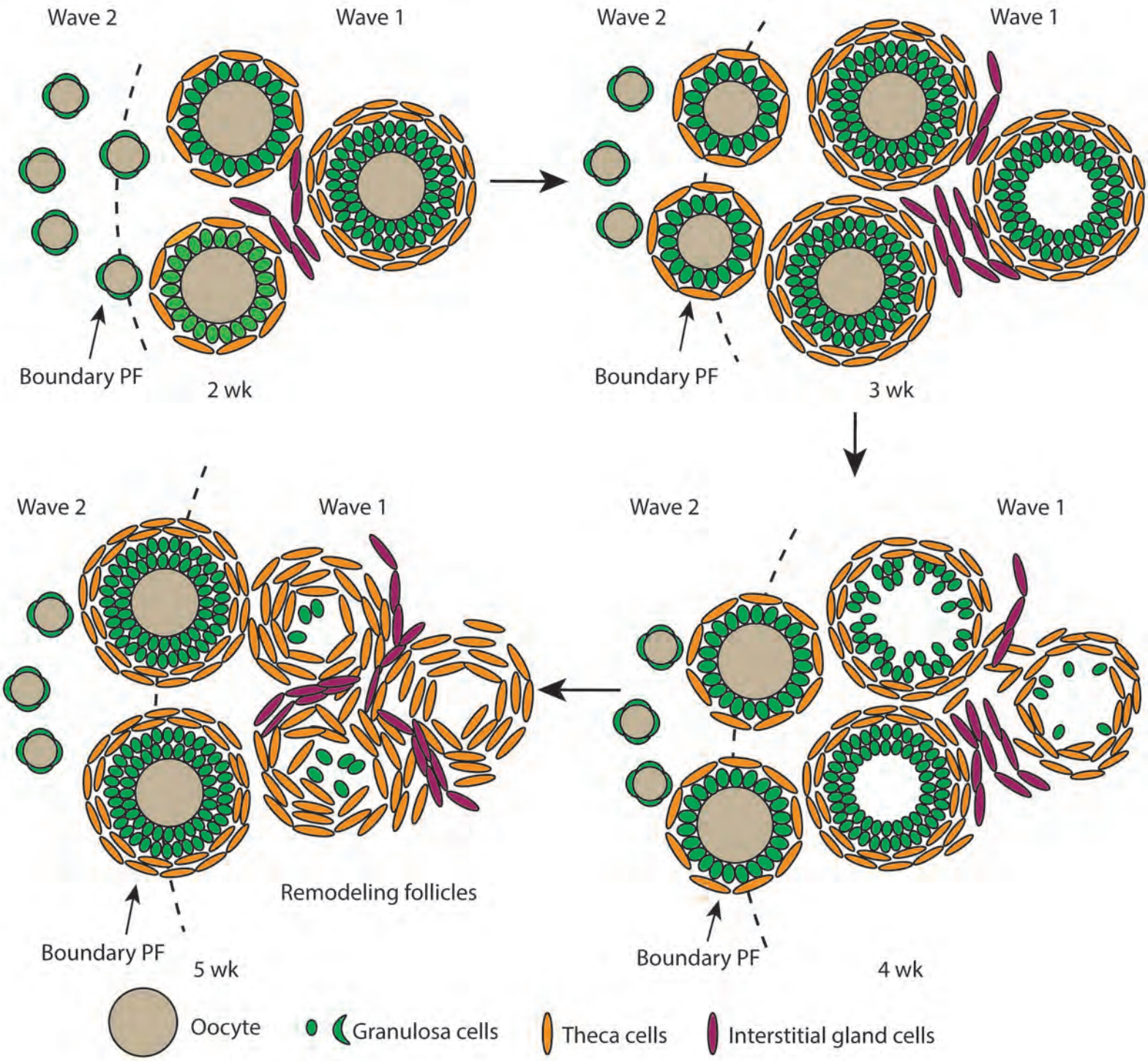
Wave 2
Wave 1
Boundary PF
2 wk
Wave 2
Wave 1
Boundary PF
3 wk
Wave 2
Wave 1
Boundary PF
4 wk
Wave 2
Wave 1
Remodeling follicles
Boundary PF
5 wk
Oocyte
Granulosa cells
Theca cells
Interstitial gland cells

Fig. S1

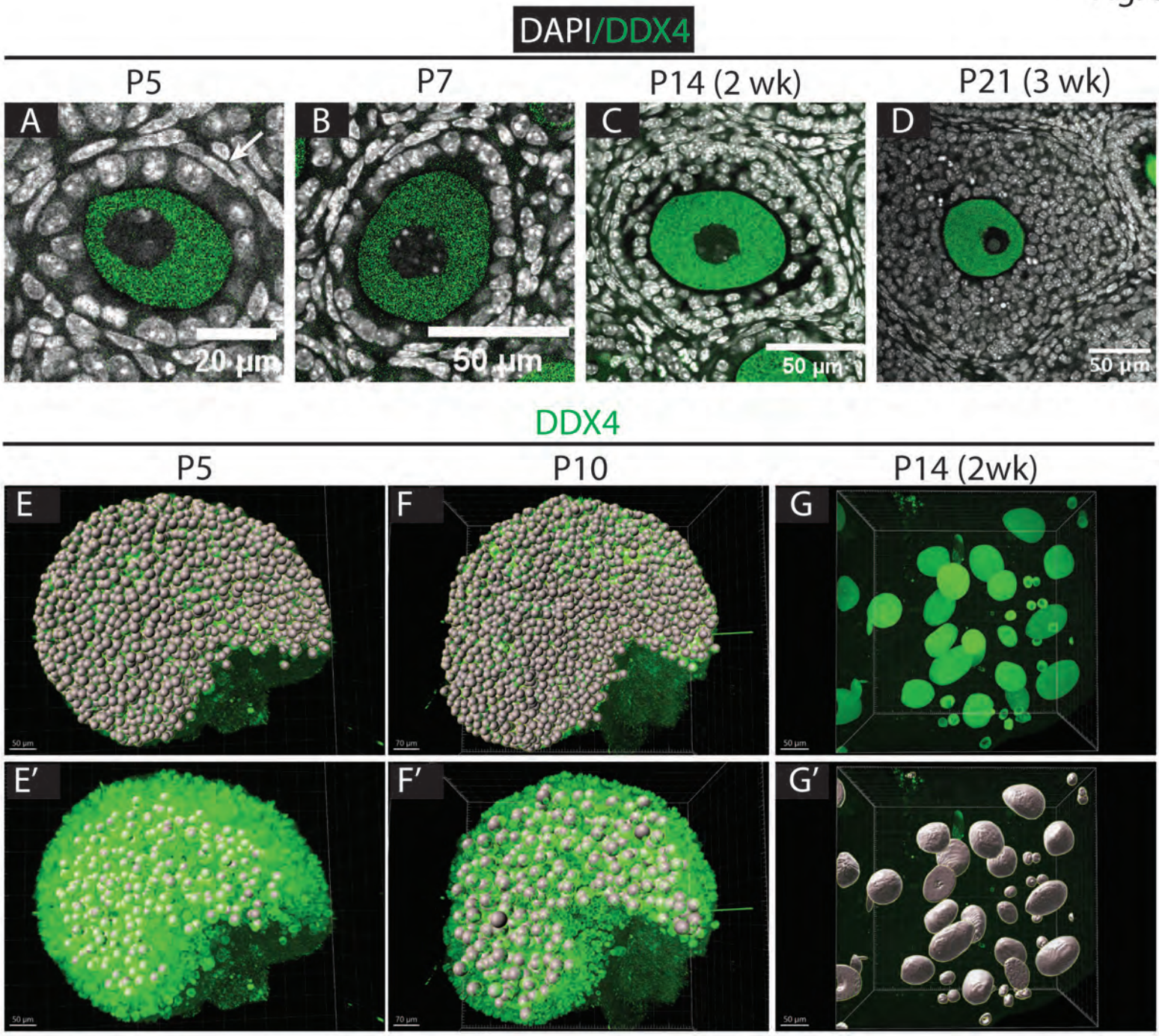
DAPI/DDX4
P5
P7
P14 (2 wk)
P21 (3 wk)
A
B
C
D
20 µm
50 µm
50 µm
50 µm
DDX4
P5
P10
P14 (2wk)
E
F
G
E′
F′
G′
50 µm
70 µm
50 µm
50 µm
70 µm
50 µm

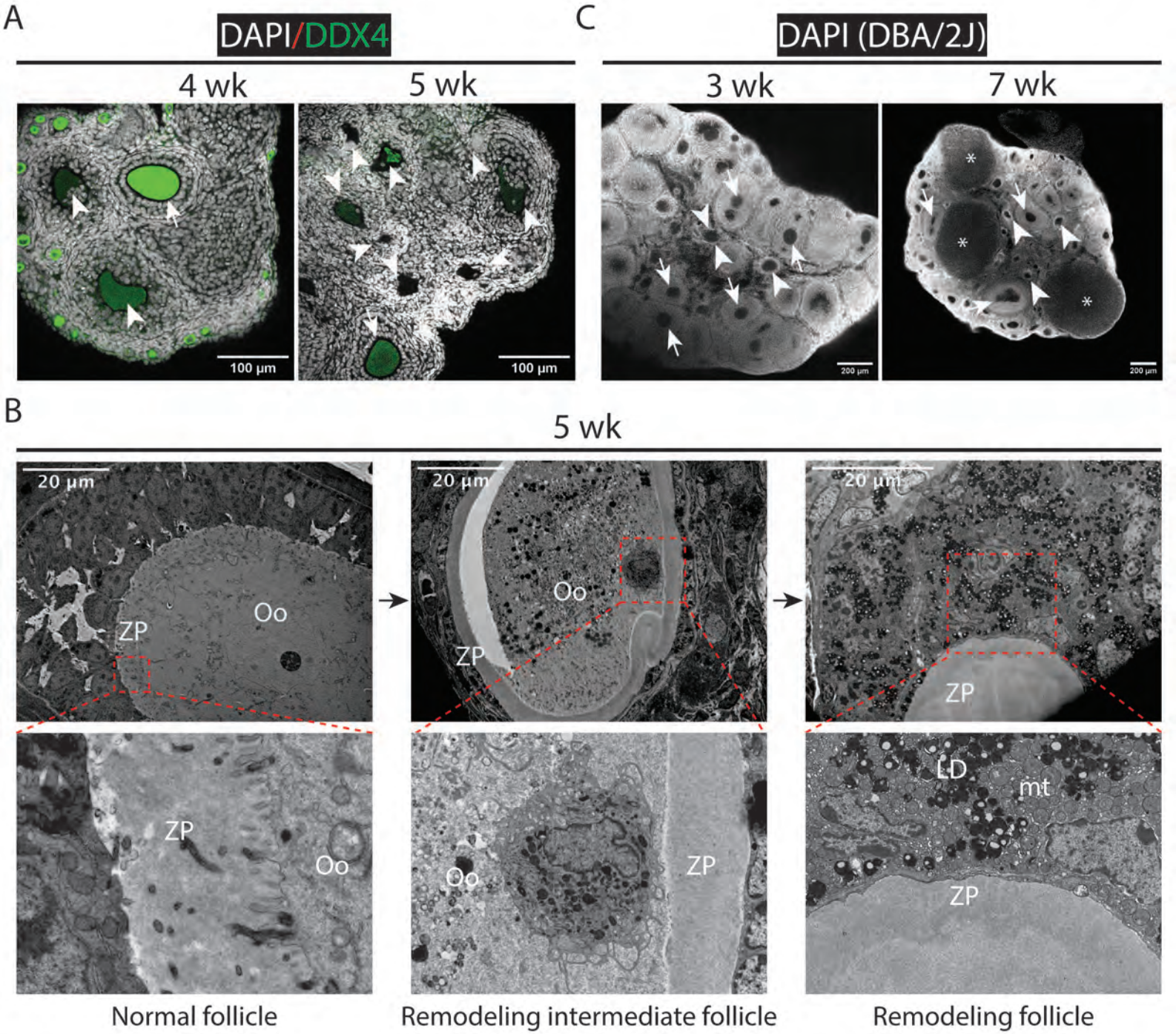
A
DAPI/DDX4
4 wk
5 wk
100 µm
100 µm
C
DAPI (DBA/2J)
3 wk
7 wk
200 µm
200 µm
B
5 wk
20 µm
20 µm
20 µm
Oo
ZP
Oo
ZP
ZP
ZP
Oo
Oo
ZP
LD
mt
ZP
Normal follicle
Remodeling intermediate follicle
Remodeling follicle

Fig. S3

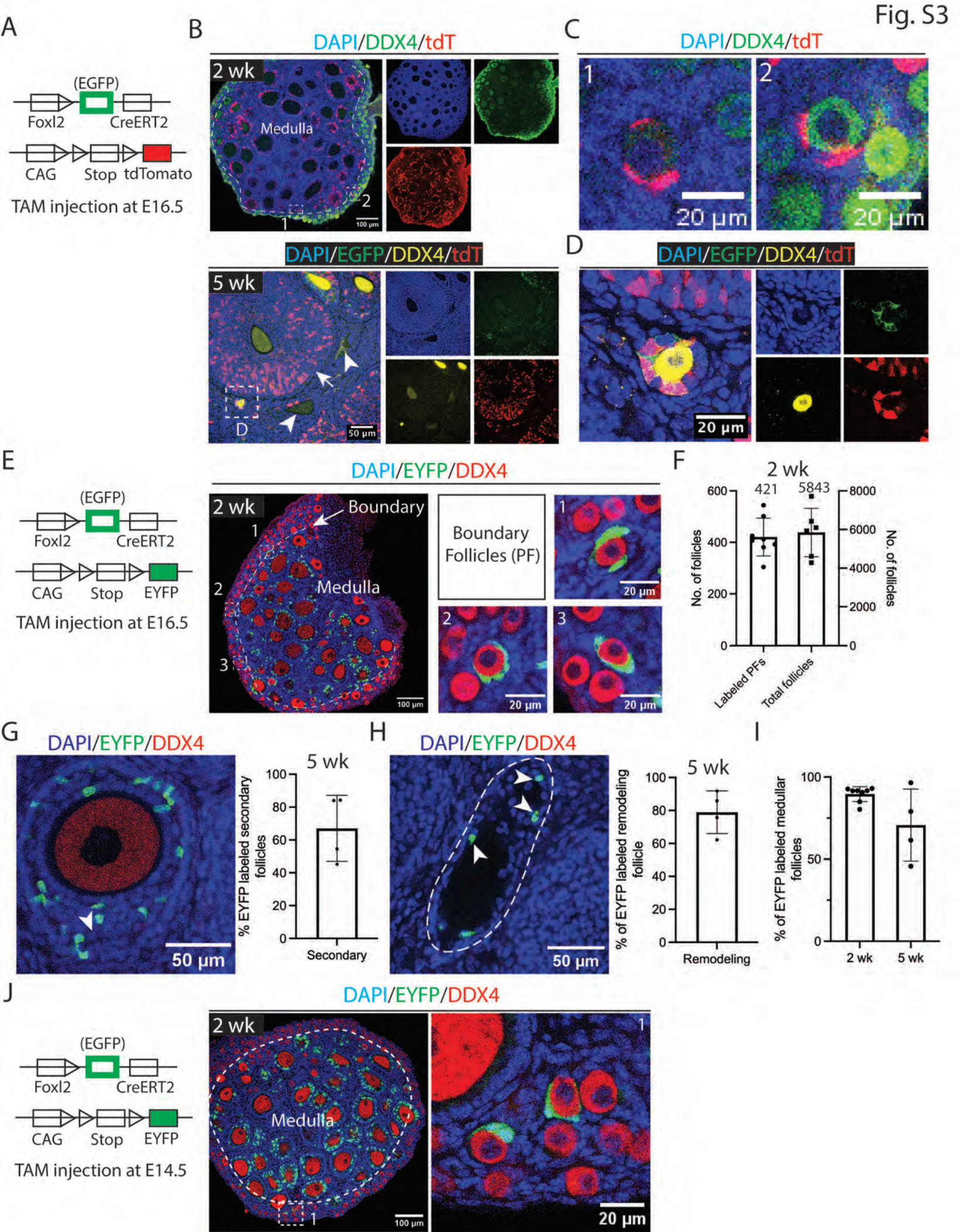
A
(EGFP)
Foxl2
CreERT2
CAG
Stop
tdTomato
TAM injection at E16.5
B
DAPI/DDX4/tdT
2 wk
Medulla
1
2
100 µm
C
DAPI/DDX4/tdT
1
2
20 µm
20 µm
DAPI/EGFP/DDX4/tdT
5 wk
D
50 µm
D
DAPI/EGFP/DDX4/tdT
20 µm
E
(EGFP)
Foxl2
CreERT2
CAG
Stop
EYFP
TAM injection at E16.5
DAPI/EYFP/DDX4
2 wk
Boundary
Medulla
1
2
3
100 µm
Boundary Follicles (PF)
20 µm
20 µm
20 µm
F
2 wk
421
5843
No. of follicles
No. of follicles
Labeled PFs
Total follicles
G
DAPI/EYFP/DDX4
50 µm
5 wk
% EYFP labeled secondary follicles
Secondary
H
DAPI/EYFP/DDX4
50 µm
5 wk
% of EYFP labeled remodeling follicle
Remodeling
I
% of EYFP labeled medullar follicles
2 wk
5 wk
J
(EGFP)
Foxl2
CreERT2
CAG
Stop
EYFP
TAM injection at E14.5
DAPI/EYFP/DDX4
2 wk
Medulla
1
100 µm
20 µm

Fig. S4

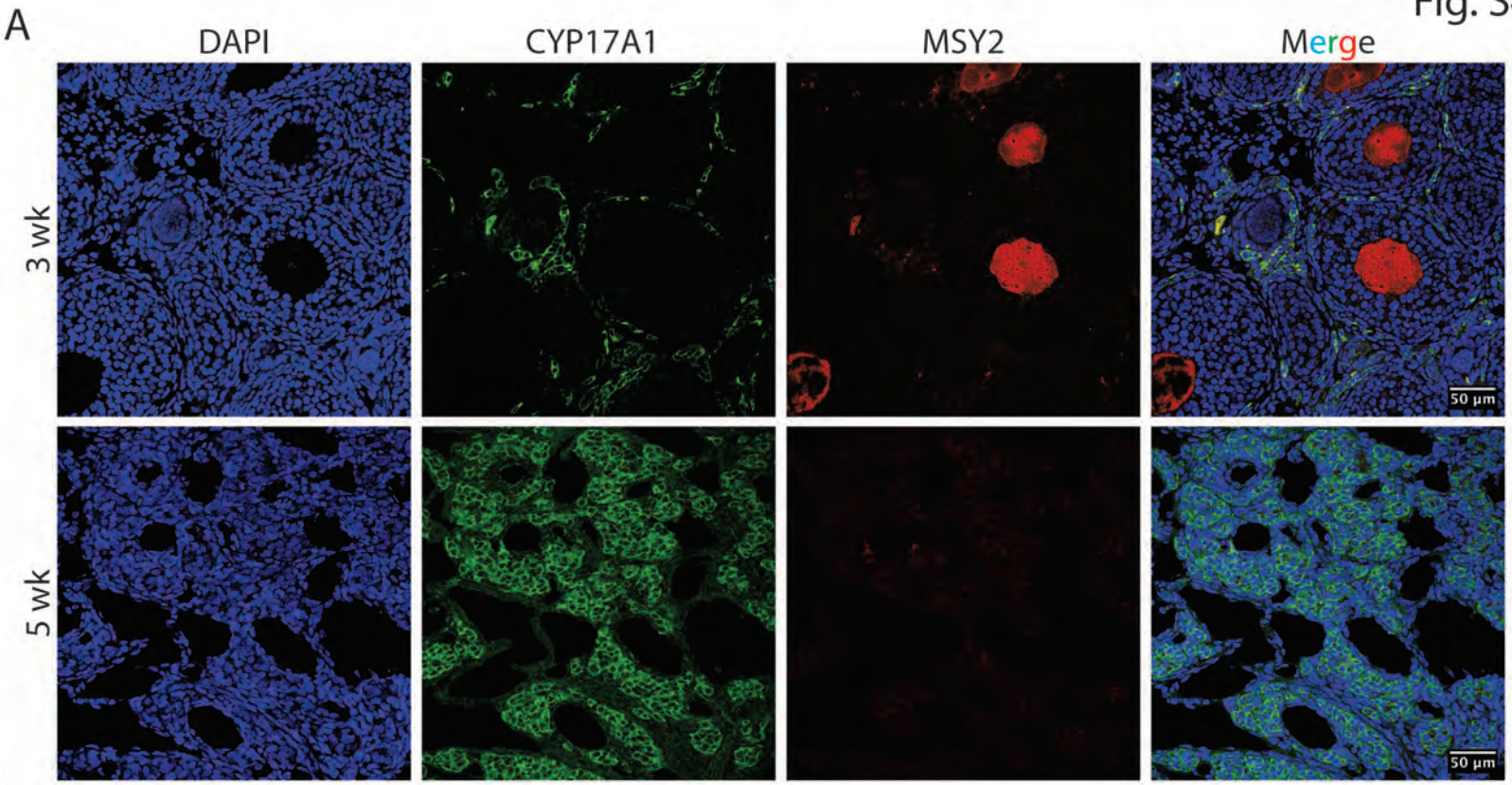
A
DAPI
CYP17A1
MSY2
Merge
3 wk
5 wk
50 µm
50 µm

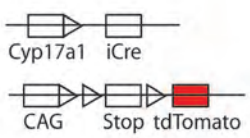
B
Cyp17a1
iCre
CAG
Stop
tdTomato

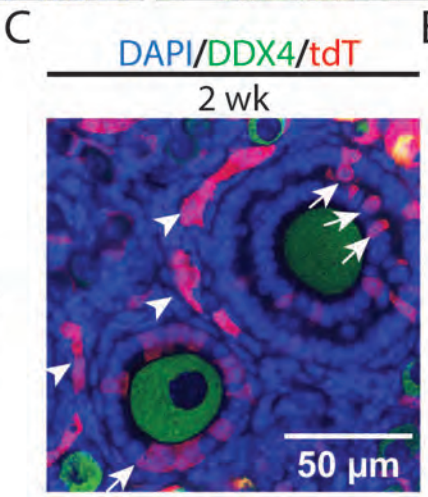
C
DAPI/DDX4/tdT
2 wk
50 µm

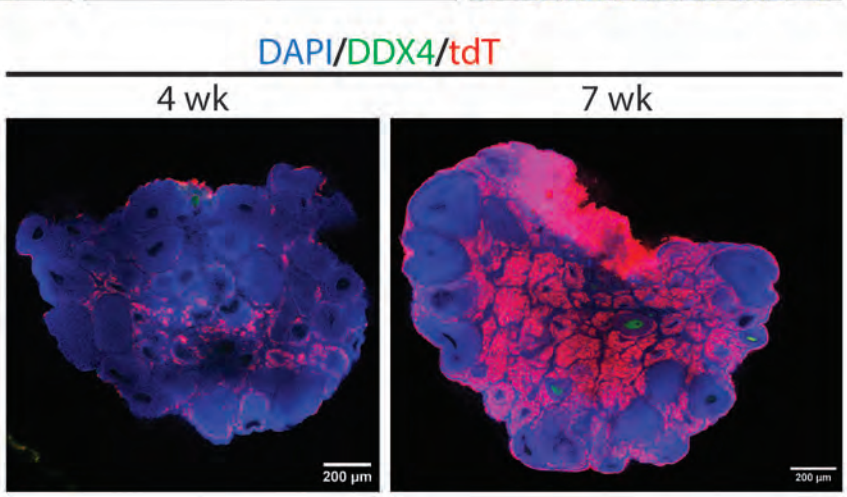
E
DAPI/DDX4/tdT
4 wk
7 wk
200 µm
200 µm

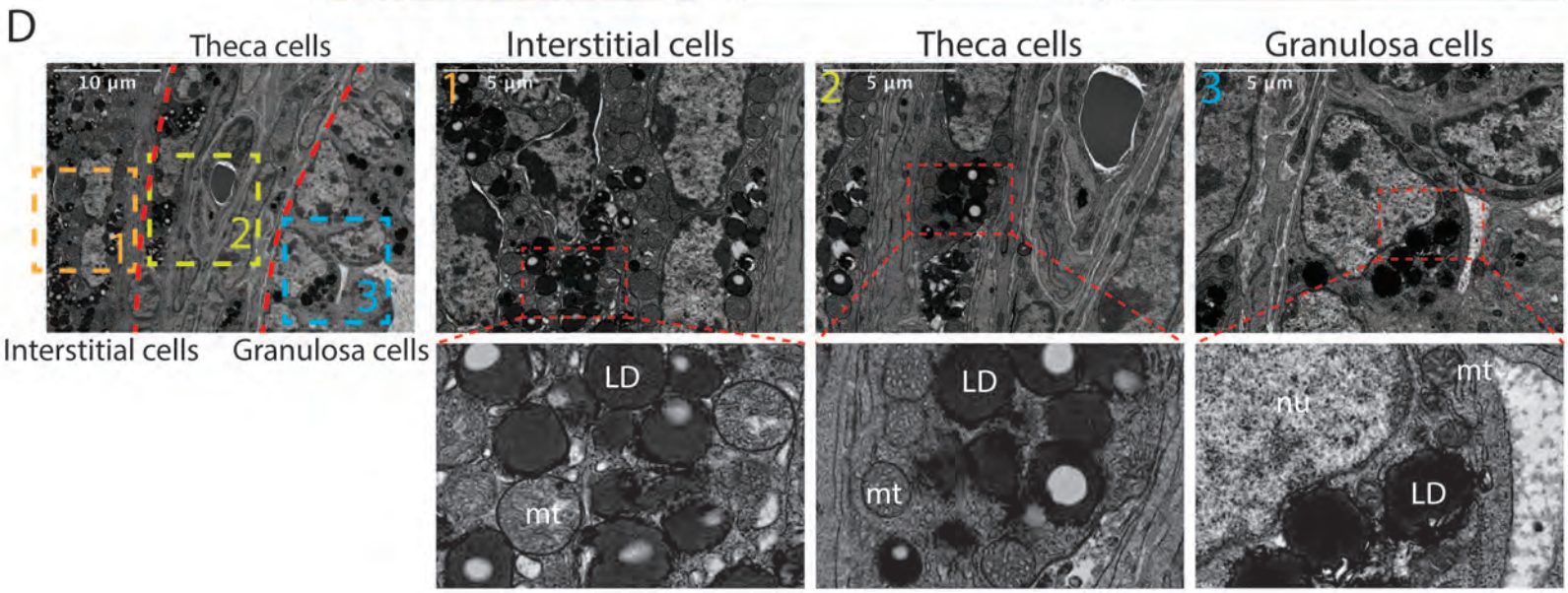
D
Theca cells
Interstitial cells
Granulosa cells
10 µm
1
2
3
Interstitial cells
Granulosa cells
Theca cells
Granulosa cells
5 µm
5 µm
5 µm
LD
mt
LD
mt
mt
nu
LD

Fig. S5

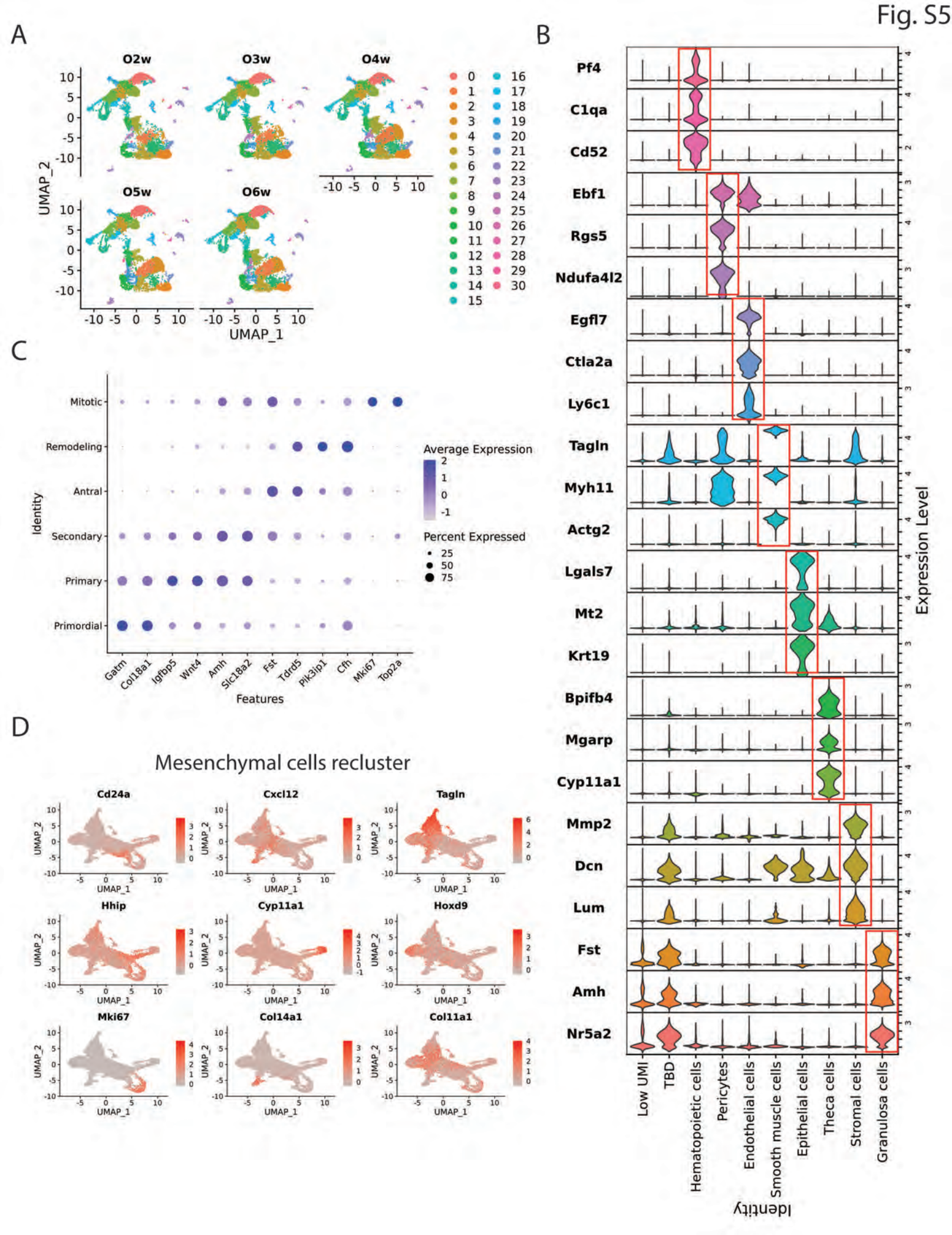
A
O2w
O3w
O4w
O5w
O6w
UMAP_2
UMAP_1
0 1 2 3 4 5 6 7 8 9 10 11 12 13 14 15 16 17 18 19 20 21 22 23 24 25 26 27 28 29 30
B
Pf4
C1qa
Cd52
Ebf1
Rgs5
Ndufa4l2
Egfl7
Ctla2a
Ly6c1
Tagln
Myh11
Actg2
Lgals7
Mt2
Krt19
Bpifb4
Mgarp
Cyp11a1
Mmp2
Dcn
Lum
Fst
Amh
Nr5a2
Expression Level
Low UMI
TBD
Hematopoietic cells
Pericytes
Endothelial cells
Smooth muscle cells
Epithelial cells
Theca cells
Stromal cells
Granulosa cells
Identity
C
Mitotic
Remodeling
Antral
Secondary
Primary
Primordial
Identity
Gatm
Col18a1
Igfbp5
Wnt4
Amh
Slc18a2
Fst
Tdrd5
Pik3ip1
Cfh
Mki67
Top2a
Features
Average Expression
Percent Expressed
25
50
75
D
Mesenchymal cells recluster
Cd24a
Cxcl12
Tagln
Hhip
Cyp11a1
Hoxd9
Mki67
Col14a1
Col11a1
UMAP_1
UMAP_2

Fig. S6

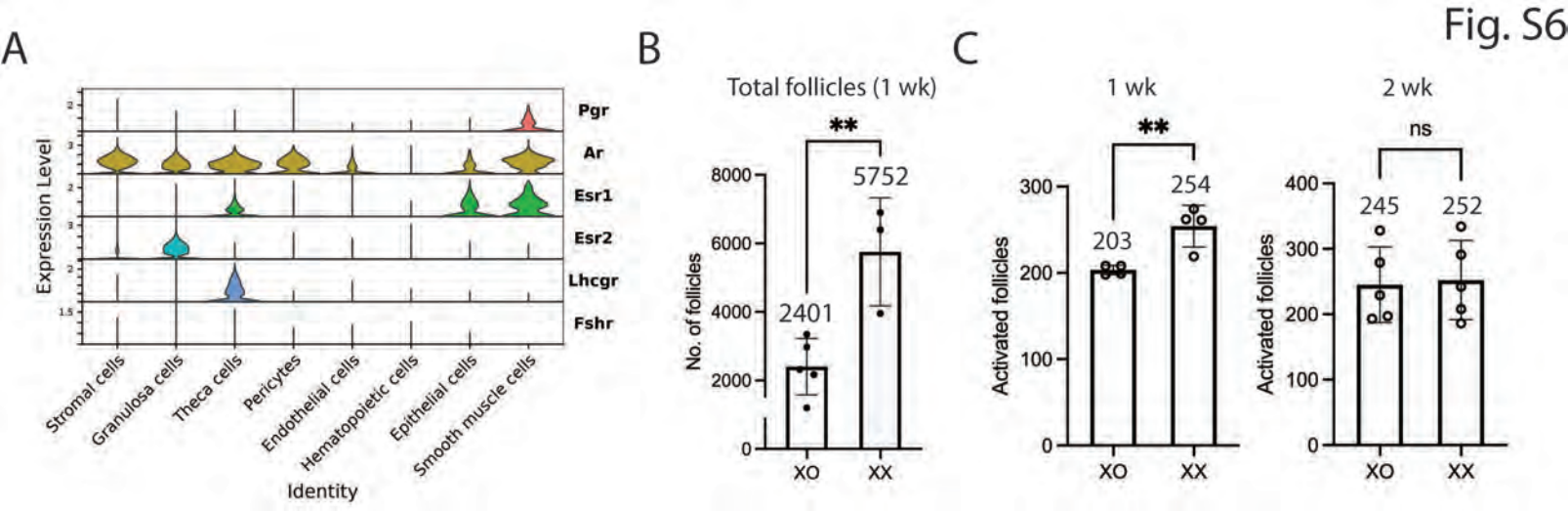
A
Expression Level
Pgr
Ar
Esr1
Esr2
Lhcgr
Fshr
Stromal cells
Granulosa cells
Theca cells
Pericytes
Endothelial cells
Hematopoietic cells
Epithelial cells
Smooth muscle cells
Identity
B
Total follicles (1 wk)
**
5752
2401
No. of follicles
8000
6000
4000
2000
0
XO
XX
C
1 wk
**
254
203
Activated follicles
300
200
100
0
XO
XX
2 wk
ns
245
252
Activated follicles
400
300
200
100
0
XO
XX